SEISMIC PRECAST

Seismic Performance Assessment of Existing Precast Industrial Buildings

POLITÉCNICO DE LEIRIA

universidade de aveiro

U.PORTO
FEUP FACULDADE DE ENGENHARIA UNIVERSIDADE DO PORTO

Past seismic events exposed important fragilities in precast reinforced concrete buildings and highlight the need to undertake measures to mitigate future losses

The study presented identify potential structural and non-structural fragilities of the Portuguese building stock and provide guidance to reduce the associated direct and indirect socio-economic impact

The project Seismic Precast

The project "SeismicPRECAST: Seismic Performance Assessment of Existing Precast Industrial Buildings and Development of Innovative Retrofitting Sustainable Solutions" was developed under the support and funding of FCT - Foundation for Science and Technology (POCI-01-0145-FEDER-028439). The project was coordinated by IPLeiria | Politécnico de Leiria, in partnership with the University of Aveiro and the University of Porto.

The research carried out aimed to contribute to the knowledge about the seismic vulnerability of existing precast industrial buildings. In particular, were obtained relevant information to perform a characterization of this type of infrastructure and the parameters that influence its response, a seismic risk study was performed, and the economic and social effects of a seismic event were assessed.

This book provides a structured overview of different project phases, from the characterization of the Portuguese precast industrial buildings stock to the risk assessment, discussing the modeling strategies and the individual building's assessment methodologies. The book also aims to promote the dissemination of the gathered results, its main reflections, and considerations.

Editors: Hugo Rodrigues, Paulo Fernandes, Romain Sousa

Authors: André Furtado, António Arêde, Fernanda Rodrigues, Hugo Rodrigues, Hugo Vitorino, Humberto Varum, Liana Ostetto, Nádia Batalha, Paulo Fernandes, Romain Sousa, Vítor Silva

Graphic design: António Costa, Sónia Morgado

Publisher: Politécnico de Leiria

DOI https://doi.org/10.25766/nhbv-9f79

ISBN 978-972-8415-05-1

Project: POCI-01-0145-FEDER-028439 - SeismicPRECAST

Founding Sources: this work was financially supported by Project POCI-01-0145-FEDER-028439 – "SeismicPRECAST: Seismic Performance Assessment of Existing Precast Industrial Buildings and Development of Innovative Retrofitting Sustainable Solutions" funded by FEDER funds through COMPETE2020 – Programa Operacional Competitividade e Internacionalização (POCI) and by national funds (PIDDAC) through FCT/MCTES.

Nádia Batalha acknowledged to FCT – Fundação para a Ciência e a Tecnologia namely through the PhD grant with reference SFRH/BD/139723/2018.

Liana Ostetto acknowledged to FCT – Fundação para a Ciência e a Tecnologia namely through the PhD grant with reference 2020.08152.BD.

Acknowledgements:

It is acknowledge the support provided by the following municipalities, to access dozens of existing design projects, enabling the characterization of the existing precast reinforced concrete building stock: Câmara Municipal de Águeda, Câmara Municipal de Aveiro, Câmara Municipal de Leiria, Câmara Municipal de Mafra, Câmara Municipal da Marinha Grande, Câmara Municipal do Montijo, Câmara Municipal de Ourém, Câmara Municipal de Porto de Mós, Câmara Municipal do Seixal, Câmara Municipal de Silves, Câmara Municipal de Sintra, Câmara Municipal de Vagos.

A special acknowledgement also to the precast companies that help us during the project, namely: Concremat - Prefabricação e Obras Gerais S.A., Mota-Engil Prefabricados, SPRAL - Sociedade de Pré-Esforçados de Aveiro Lda, Verdasca & Verdasca S.A., Vigobloco - Pré-Fabricados S.A., VEconcept.

Table of Contents

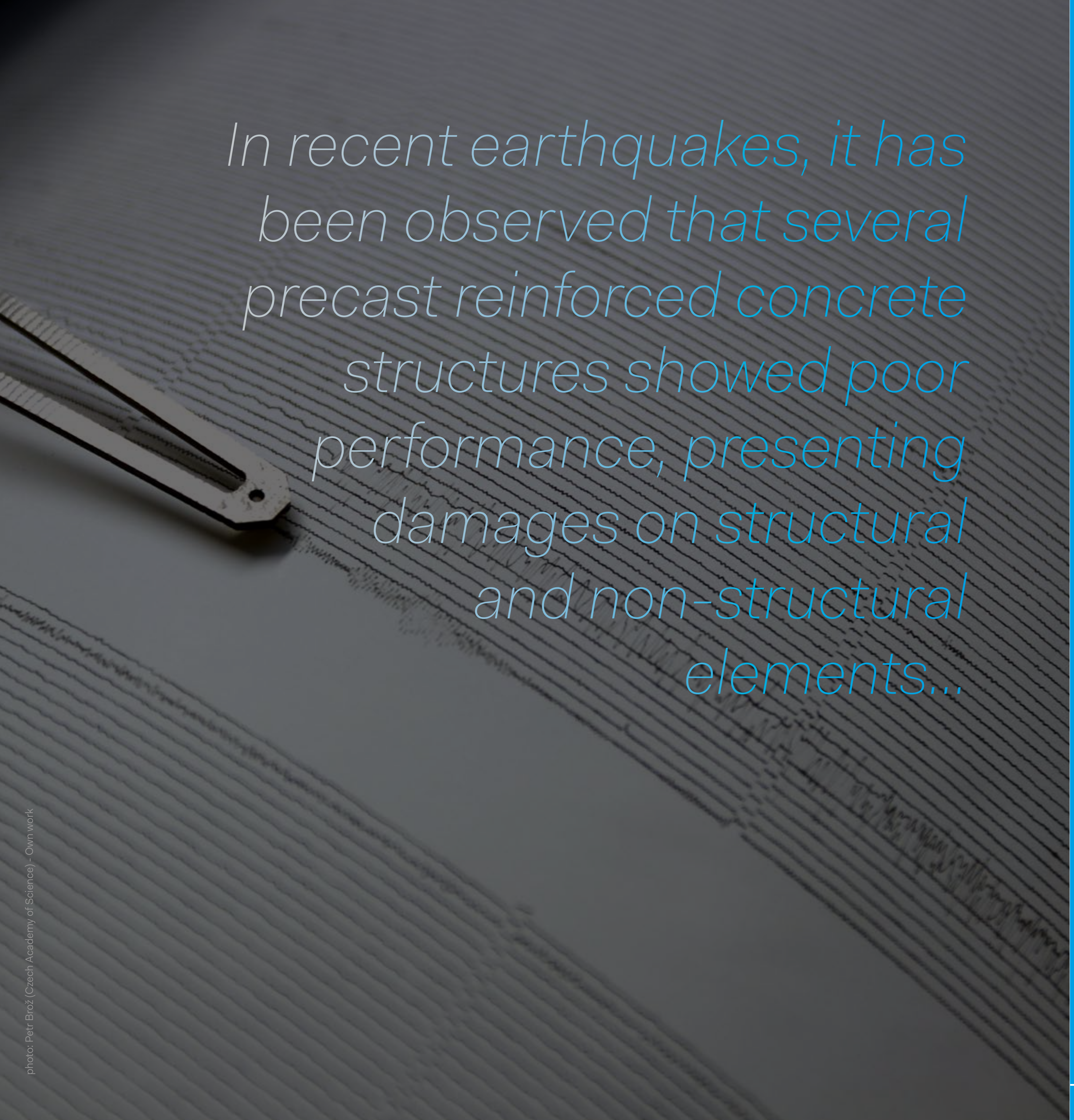

photo: Petr Brož (Czech Academy of Science) - Own work

1. Introduction

Nowadays the constitution of industrial buildings are essentially based on precast reinforced concrete (PRC), steel, and mixed steel-concrete structures [1]. In recent earthquakes, it has been observed that several PRC structures showed poor performance, presenting damages on structural and non-structural elements, highlighting the vulnerability of industrial buildings, in particular the ones designed without seismic provisions [2]–[5]. In several buildings were observed significant failures and collapses. For example, in the Emilia-Romagna (Italy) earthquake of 20th and 29th of May 2012, more than half of the existing precast structures exhibited significant damage [6]–[8]. Even in moderate and short duration earthquakes events, precast reinforced concrete structures exhibit high levels of structural damages as Romão *et al*. [9] described after field observations of the 2011 Lorca earthquake, in Spain. The damage reported after different seismic events pointed to the need for consistent methodologies for the analysis, modeling, and assessment of the existing precast reinforced concrete constructions located in seismic-prone regions. Those models need to account for the interaction between structural elements (e.g., beam-to-column connections) and structural and non-structural elements to describe the non-linear dynamic behavior of this type of structure [10]–[13].

In this context, the research project SEISMICPRECAST emerged to identify the seismic vulnerabilities of the Portuguese precast reinforced concrete building stock and provide useful guidelines for the modeling, design, and assessment of buildings in order to mitigate the potential socio-economic impacts from future seismic events.

After a comprehensive description of damage observed in previous earthquakes (Chapter 2), this document describes the main properties of the Portuguese building stock (Chapter 3), with particular attention to the experimental and numerical characterization of the beam-to-column connections with different configurations (Chapter 4) and its influence in the overall building performance (Chapter 5). The information collected in the previous tasks was critical to conduct the seismic assessment of existing precast reinforced concrete buildings according to the Eurocode 8 – Part 3, which is the current code in practice for the seismic assessment of existing buildings (Chapter 6) and to perform the seismic risk analysis that enables the estimation of the direct and indirect losses associated with this typology of buildings for two seismic scenarios compatible with the Portuguese seismic hazard (Chapter 7). A summary of the main findings is presented in Chapter 8.

2. Observed damages in recent earthquakes

The most common structural damages are observed in the columns, beams, and connection elements.

Starting with the columns, the most common failures observed during field surveys were the: i) failure at the base of the columns (development of a plastic hinge) [4], [14]–[16]; ii) short-column failures [4], [16], [17]; and iii) failure at the top [4], [16]. Liberatore *et al.* [4] showed with their research that almost 50% of the industrial buildings presented severe damages.

The formation of a plastic hinge at the base column is a common damage in PRC structures. Liberatore et al. [4] referred that more than 40% of the buildings investigated due to Emilia earthquakes in 2012 were damaged with a plastic hinge at the column. Also, Posada & Wood [14] referred to a plastic hinge at the base of a precast column as frequent structural damage. Casotto et al. [18] referred to plastic hinges as a result of the inadequate column cross-sections, namely in the out-of-plane direction. Figure 1a) illustrates a detail of a plastic hinge with bars buckling, while Figure 1b) illustrates severe concrete detachment, probably due to the plastic hinge. Another cause of column rotation is foundation rotation due to inadequate column-to-foundation connection [5]. Savoia et al. [19] referred that the industrial building with pocket foundations, widely used after the '90s, do not have any connections between the precast column and the cast-in-situ foundations. The author also refers that the wind was the only horizontal action in the design stage of these foundations. Another cause of column rotation is foundation settlements or failure of the precast sleeve footing. Despite saving time of construction, this technique already showed that does not exhibit any overstrength capacity when the external bending moment overcomes the stabilizing moment [15]. In these cases of column rotations, RC pavements have a favorable role in avoiding excessive column rotation and the consequent falling of the upper beam.

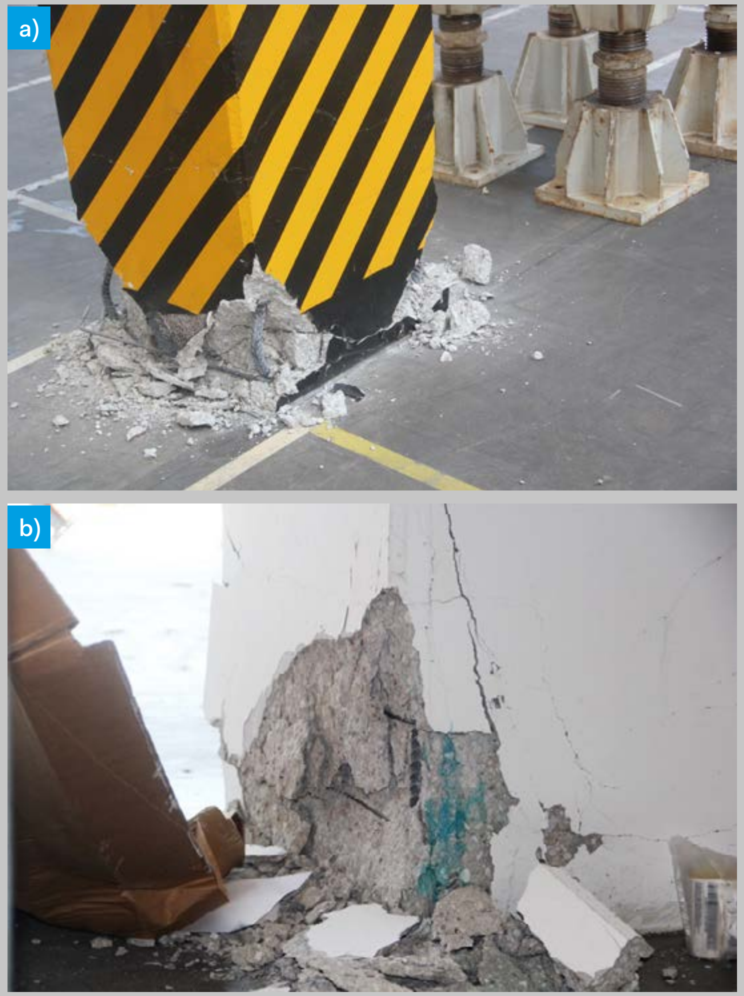

a) Plastic hinge with bar bucking on a central column

b) Spalling

Figure 1 · **Examples of plastic hinges on columns**

Another damage related to columns failure is the short-column effect. This phenomenon is caused due to the arrangement of infill panels, adjacent new constructions without an adequate seismic joint, contiguous hall with different weights (Figure 2), or sawtooth roofs with inclined beams [4], [17]. Indeed, the most frequent cause of damage related to short-column is related to industrial buildings with strip windows on top of curtain masonry walls/cladding panels.

Analyzing the top of the columns, local damages are common. According to Liberatore et al. [4] there are two types of column top damages: i) spalling of the concrete that is directly supporting the beam; and ii) failure of the lateral cantilever (forks) that laterally restrict the beam (Figure 3).

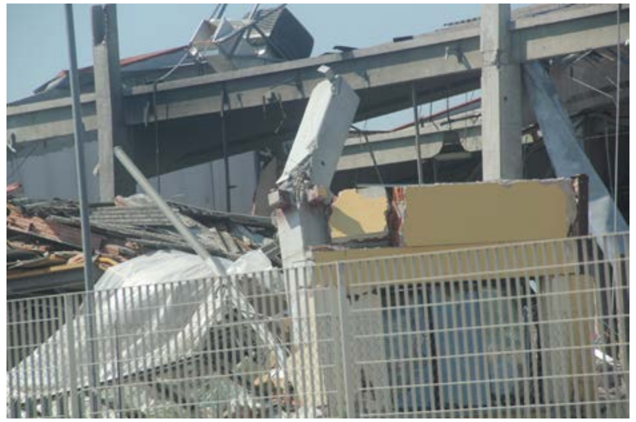

Figure 2 · **Short-column effect due to the interaction with irregular masonry walls**

Figure 3 · **Collapse of the forks at the top of the columns due to out-of-plane actions**

The spalling of the concrete is due to a strong steel bar placed in a weak RC element or placed with a small concrete cover or even to a thick layer of fire protection or due to the lack of neoprene pad on the interface between the concrete elements [20]. The failure of the lateral cantilevers that restraints the pocket support, which is a more common failure, is associated with the unseating of the beams from the top of the columns. This loss of support is more common in the central column due to the limited length of support and, in an earthquake event, the displacement between the beam and the column exceeding the available length leads to the beam's fall [6]. Figure 4 shows an example of the loss of support from the column due to the support forks failure.

Regarding the observed beam damages, compared to what has already been documented, beam failure is not very common. In fact, the main cause of beam failure is related to the loss of support (see Figure 5). The absence of a proper beam-to-column connection, which could also prevent the spalling between the column and the beam, is the main reason for the beam collapses [4], [15].

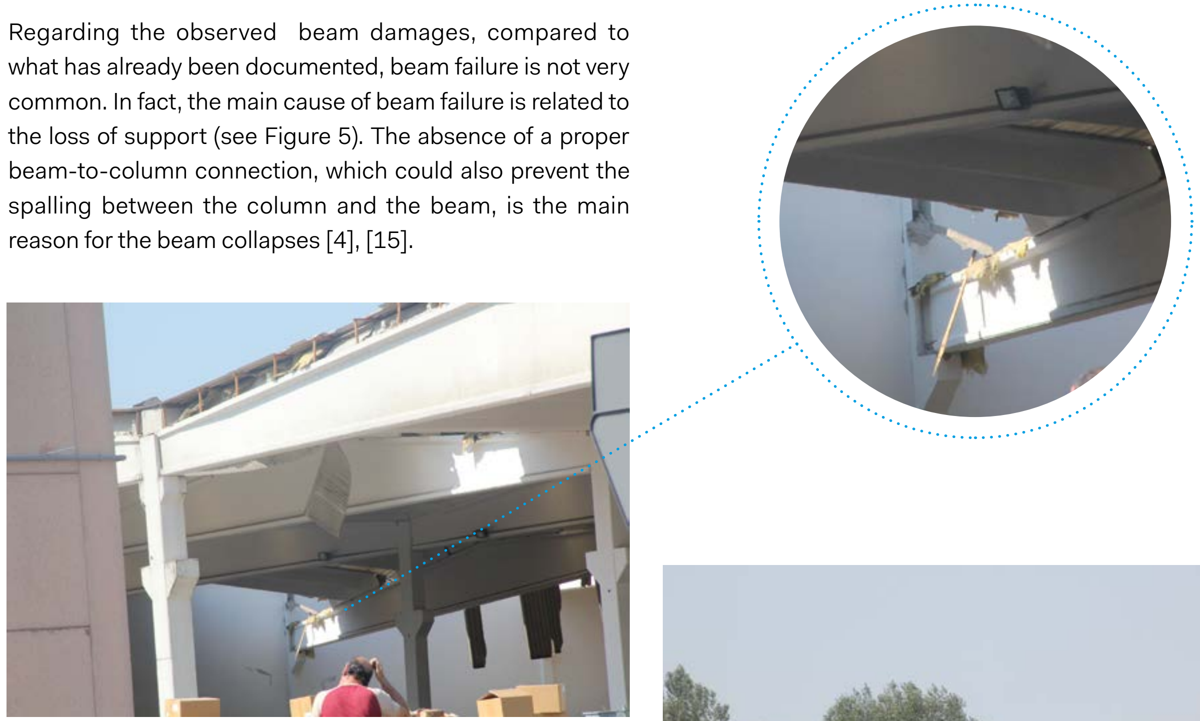

Figure 4 · **Loss of support of the beam from the column**

Figure 5 · **Failure due to loss of support of the beam**

Another problem associated with beams is their rotation, as illustrated in Figure 6. This problem is associated with roof panels, more specifically with the lack of connection. In many cases, the roof's collapse is a consequence of the beam failure [5]. Bournas *et al*. [6] reported that 25% of PRC industrial buildings designed with no seismic provisions presented partial or total collapse of the roof and girders.

Finally, regarding the structural elements, the connections are the most crucial elements on PRC structures and, as such, are the main source of building failure, as reported by several authors [2], [5], [6], [16], [21]. The most critical failures related to connections were those between i) beam-to-column; ii) roof-to-beam; iii) column-to-foundation; and iv) cladding panel-to-structural element. Belleri *et al*. [2] refer that the most severe structural damage that occurred during the Emilia earthquakes are related to the beam loss of support and consequent falling due to the lack of mechanical connection (dowel) as a seismic load transfer mechanism between beam-to-column and roof-to-beam. This type of collapse affected more significantly structures built in the '70s and '80s. Figure 5 presents a good example of beam-to-column inappropriate connection and consequent loss of roof elements' support. Bournas *et al*. [6] referred to the key issue of beam-to-column connections the ability to allow relative displacements without losing beam seating or to properly transfer lateral horizontal forces to the column and down to the foundation without losing capacity.

Regarding the roofs, the flexible ones are the most used due to the absence of mechanical connections between the joints, so the seismic actions are directly transferred to the primary beams, which in some cases exceed their own out-of-plane capacity and collapse. Figure 7 illustrates beam damage due to the roof-to-beam connection.

Figure 6 · **Rotation of the beam**

Figure 7 · **Beam damage due to the roof-to-beam connection**

It has been observed in past earthquakes that PRC buildings exhibited poor performance, with severe damage on structural and non-structural elements, highlighting the vulnerability of these industrial buildings [2], [4], [5]. Particular attention has been given, by different authors [4], [6], [19], to the non-structural damages, in particular to the storage racks failures, whose source of failure is associated with the lack of proper design for earthquake loads and the inadequate longitudinal bracing [5], [22].

However, regarding the non-structural damages, the failure of cladding panels is the most documented one in PRC industrial buildings, with several authors reporting heavy damages [4], [5], [19], [23]. In particular, Bournas *et al*. [6] reported that approximately 75% of precast industrial buildings designed without seismic provisions exhibited damage and detachment of the exterior claddings' panels. In Italy, Liberatore *et al*. [4] highlighted that 50% of the industrial buildings presented severe damages in the cladding elements and infill panels in the 2012 Emilia-Romagna earthquake.

Some of the critical problems reported in recent earthquakes in Italy are associated with the cladding-to-structure devices used in the past [24]. The observed damages in cladding panels are mainly related to the failure of the fastening elements and the consequent out-of-plane overturning [4]. Figure 8 represents details of the detachment of a horizontal cladding panel connection like typical connections found in Portugal. The most current arrangement of cladding panels observed in PRC buildings in the Portuguese industrial park is the horizontal ones [25], identified by several authors [2], [26], [27] as the most vulnerable one.

Figure 8 · **Top view of the cladding-to-column connection failure [16]**

The cause of the failure of cladding panels is mainly related to the development of in-plane forces, typically not considered during the design process [28]. These forces arise due to the high in-plane stiffness of these walls, which is ignored during the design process. The current design practices [29], [30] assume cladding panels as non-structural elements, neglecting their contribution and interaction with the structure. A recent survey carried out in Portuguese PRC buildings [25] found that cladding panels, both in old and new buildings, are generally not considered in the design, not even with simplified procedures, considering that they do not contribute to seismic behavior. In fact, the design only considers the panels' mass while considering a bare frame structure. Under earthquake loads, the panels are then subjected to in-plane forces greater than expected, exceeding the shear capacity of the fastenings [28].

The previous considerations highlight that ignoring these elements' contribution may lead to the serious collapse of these types of elements (Figure 9) and represent a potential hazard for humans and huge economic losses [16], [23]. Moreover, the different cladding-to-structure fastenings play a key role in the safety, performance, and economics of the cladding system as well as the main structure itself.

Figure 9 · **Example of a collapsed cladding panel after the 2012 Emilia-Romagna Earthquake in Italy**

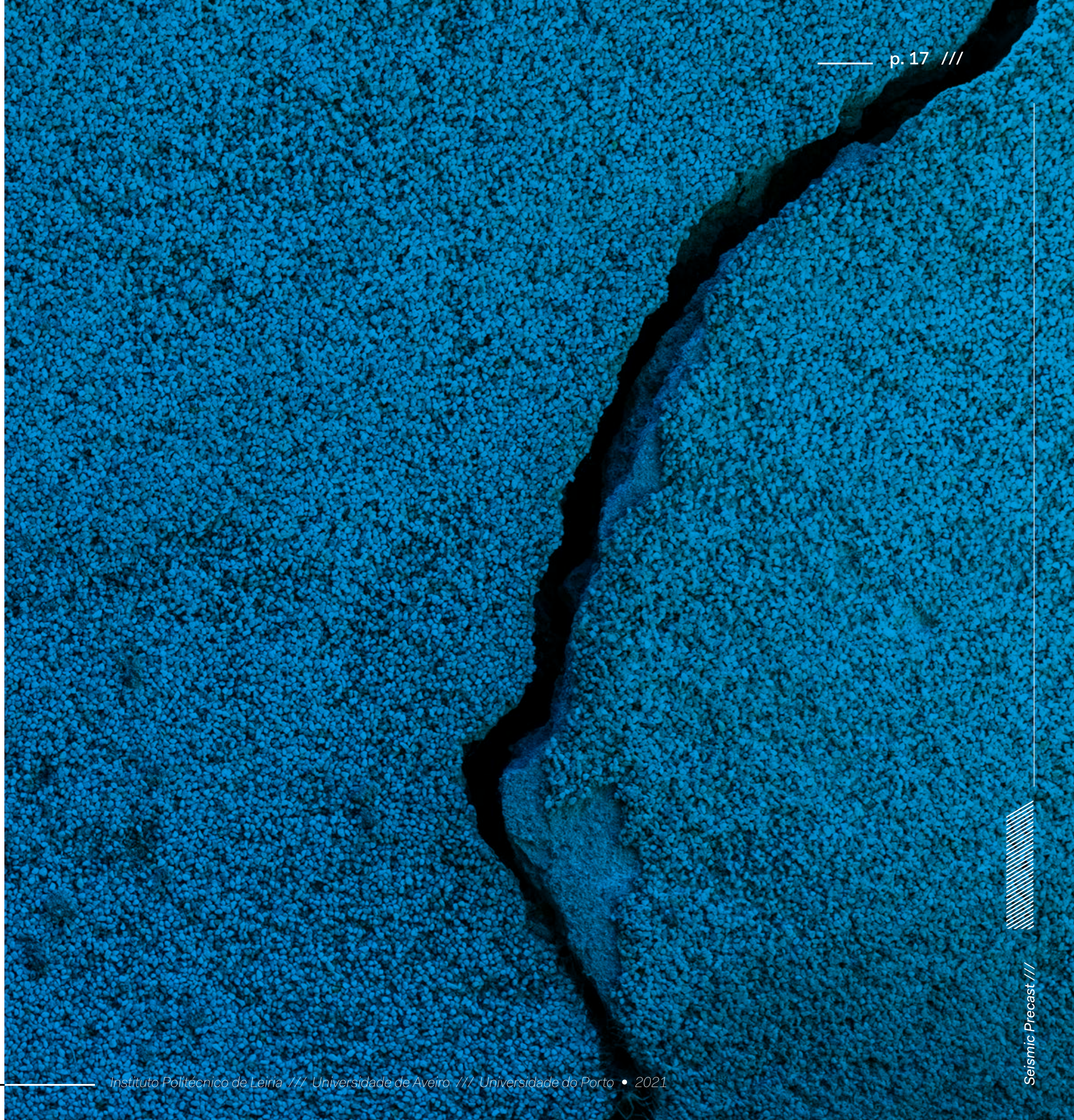

3. Characterization of the Portuguese Industrial Building Park

Contrarily to what is observed for residential buildings, limited information is available regarding the properties of precast buildings. To overcome the previous limitation, a survey was carried out analyzing the structural design project of dozens of industrial PRC buildings built in the Portuguese continental territory over the last 50 years. It should be noted that these buildings represent only a fraction of the total industrial facilities in Portugal, as depicted in Figure 10a).

Despite not being directly linked to the building's characteristics, the type of activity developed (Figure 10b) indicates the size of the buildings and type of load admitted in the design process, which may condition the size of the structural elements. For example, in heavy industries, the presence of large capacity cranes is expected, as opposed to what is expected, for example, in warehousing buildings.

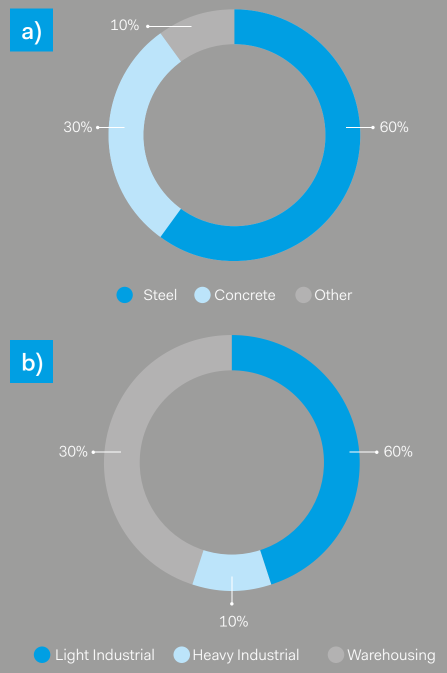

Figure 10 · **Characterization of the industrial buildings in Portugal: a) Structural typologies [31] and b) main activities developed**

Focusing more specifically on the PRC buildings, the statistical analysis of the information collected enabled the characterization of the global geometry and the mechanical properties of the materials, as well as other local systems that may influence the seismic response of these buildings, such as columns size and reinforcement ratios, beam-to-column connection and cladding systems.

The database presented in this chapter was built based on the information collected after analyzing 73 design projects of existing PRC buildings in the Portuguese mainland. The identification of the buildings sought to reflect an adequate geographical and temporal representation. Regarding the geographical distribution, Figure 11 compares the location of the collected projects and the actual manufacturing industry according to the data available in Pordata [32].

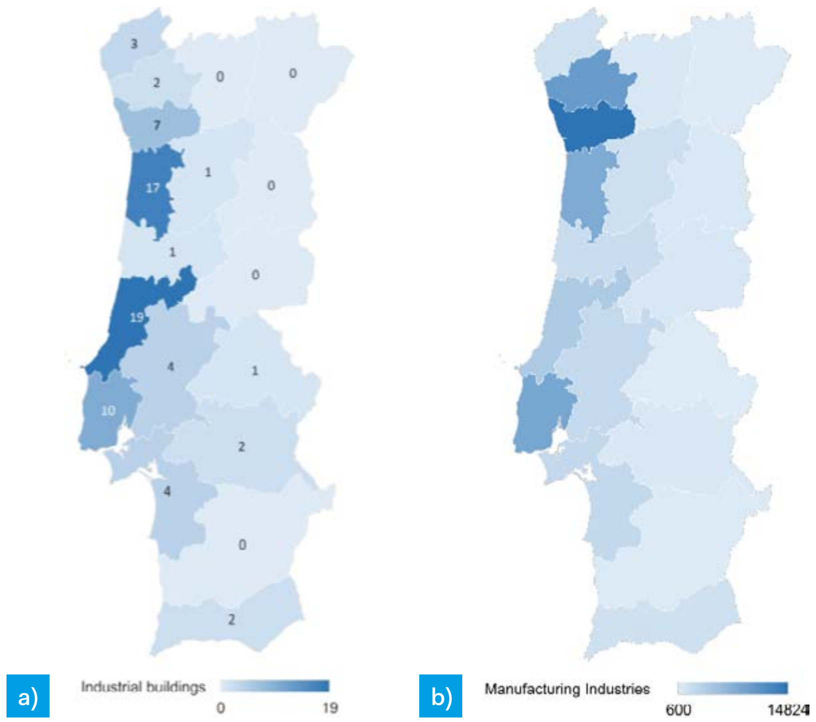

Figure 11 · **Location of industrial buildings in Portugal: a) collected projects and b) manufacturing industries in 2017**

Regarding the construction period, the buildings analyzed were built over the last 50 years and show a clear concentration after 1990 (Figure 12 a). The first reason for this concentration is related to the very limited, or absence, of information in the design project of older buildings. Moreover, until the '60s, the precast industry in Portugal was mainly focused on producing elements for slabs and cladding panels. It is only during the '70s that an important growth in the precast systems could be observed [33]. Figure 12 b) also shows the correlation between the year of construction and the seismic zones, showing that, for the buildings consulted, there is a tendency for a concentration of newer structures in the higher seismic zones (lower seismic hazard).

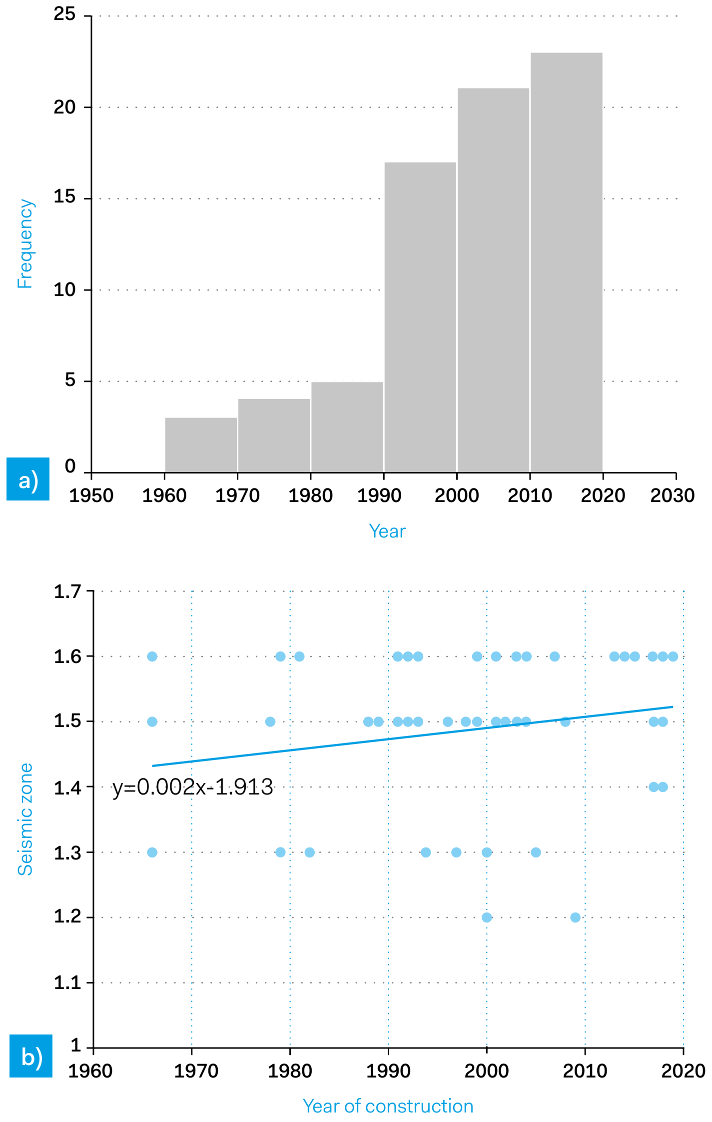

Figure 12 · a) Distribution of number of buildings analyzed by the year of the project;
b) Evolution of the seismic zone with the year of the project

Based on the survey carried out it was possible to verify that one typology stands out with more than 5/6 of all the different typologies identified, following closely the sketch illustrated in Figure 13. This typology is characterized by having one-storey with parallel portals with fixed columns at the base and pinned/friction beam-to-column connection.

In what regards the number of storeys, it is apparent that the majority of the precast buildings are single storey buildings (Figure 14 a) with a total height that is below 10 m for the majority of the cases (Figure 14 b), that is in line with the study conducted by [31] for the general industrial facilities in Portugal.

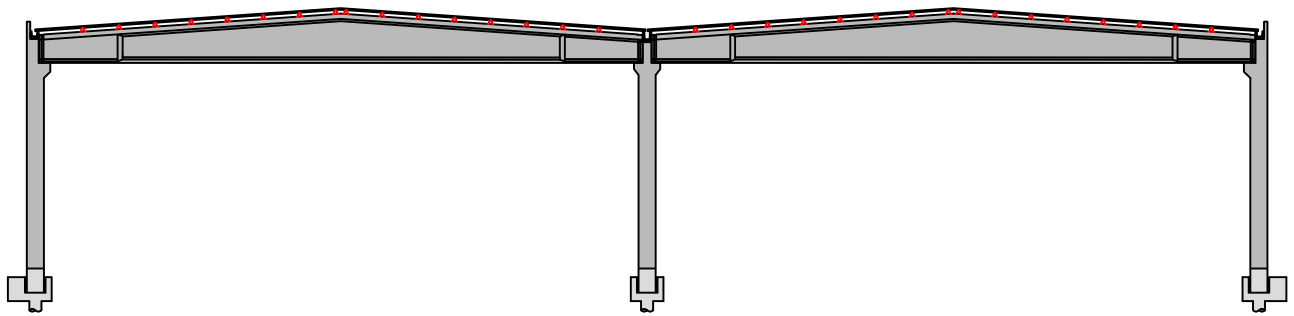

Figure 13 · Illustration of the main PRC typologies identified in Portugal with a variable cross-section I shaped prestressed beams

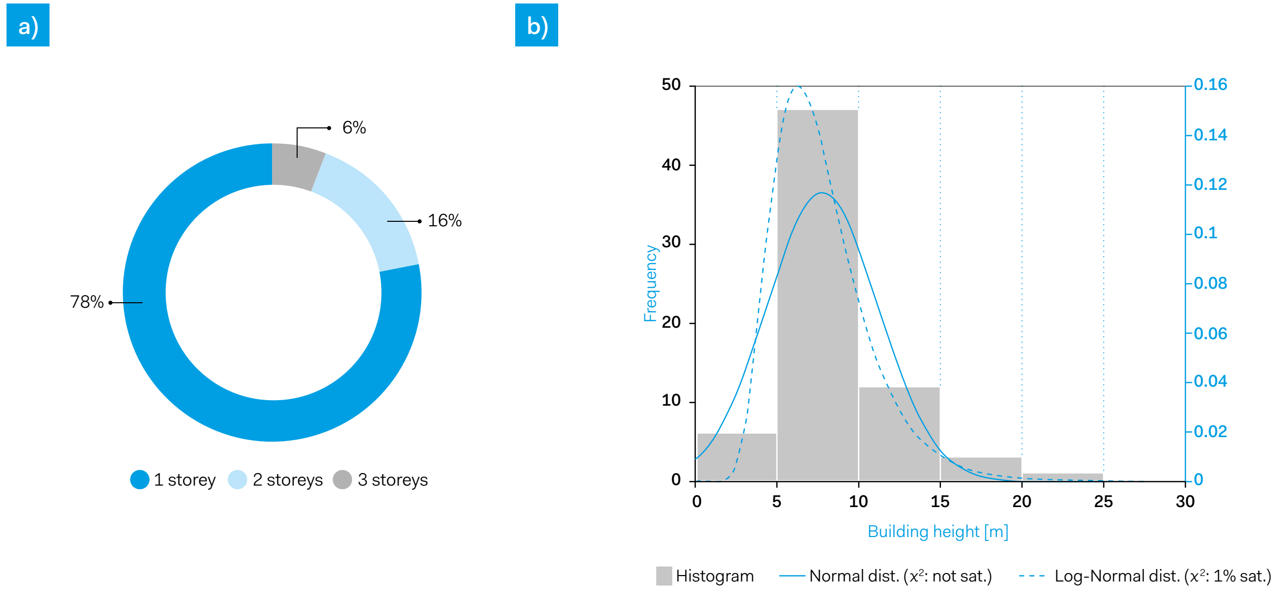

Figure 14 · **a) Number of storeys; b) Histogram and probability distributions associated with the building height**

In terms of plan geometry, the properties vary significantly depending on the building direction analyzed. In the direction along the longer beams, the number of spans is generally low (1 or 2), and the length of the beams can reach values up to 50 m (Figure 15). In addition, when analyzed with respect to the construction period, the length of the spans seems to increase with the year of construction, probably related to improvements in the manufacturing and construction processes. On the other hand, in the transverse direction, the number of spans is typically higher and features smaller lengths, up to 15 m (Figure 16).

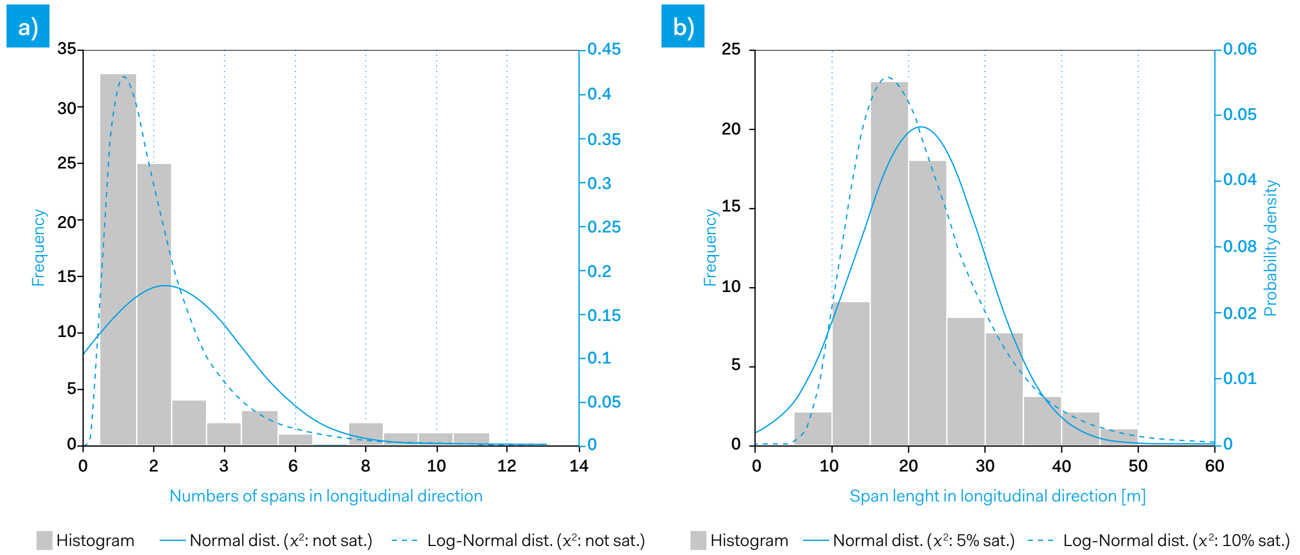

Figure 15 · **Histogram and probability distributions associated with the: a) number and; b) length of the spans (in the longitudinal direction)**

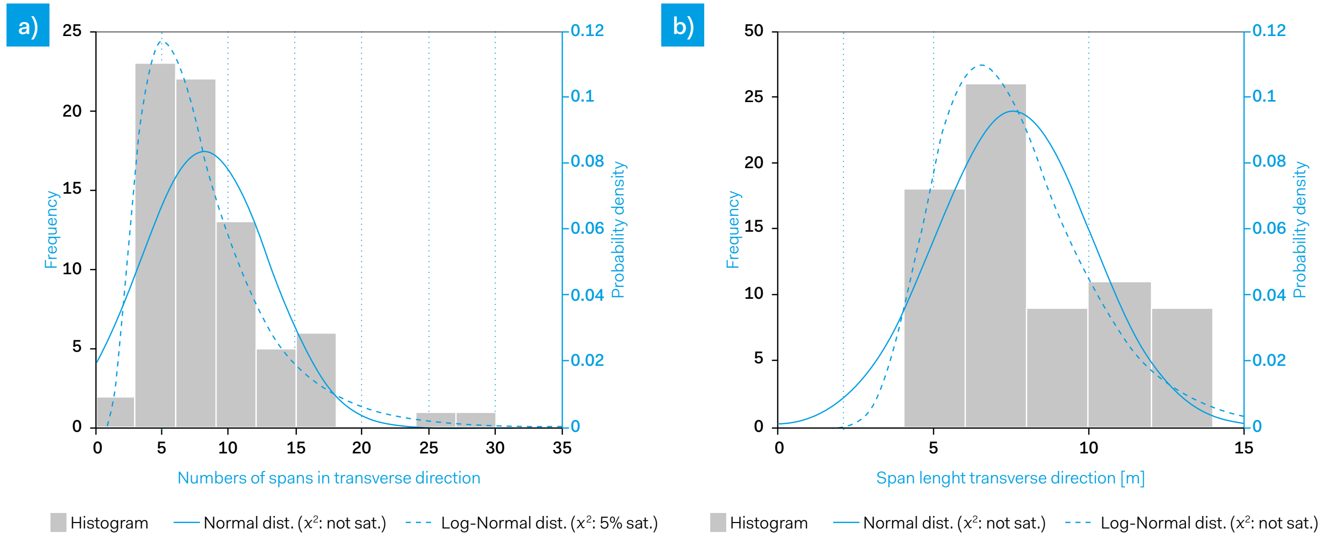

Figure 16 · **Histogram and probability distributions associated with the: a) number and; b) length of the spans (in the transverse direction)**

Finally, based on the data collected, three main types of cladding systems were identified: infill masonry, horizontal and vertical PRC panels. Among these, the use of horizontal panels seems to be most common, being observed in 50% of the buildings, while infill masonry and vertical panels were identified in 33% and 17% of the cases, respectively. The increase in the use of vertical cladding panels in the last decades (Figure 17) indicates that this solution appears to become more appealing due to improved precast construction processes, transport and installation methods. On the other hand, it is still somehow surprising that infill masonry represents a significant percentage of the buildings in the last decade and about one-third of the total number of buildings.

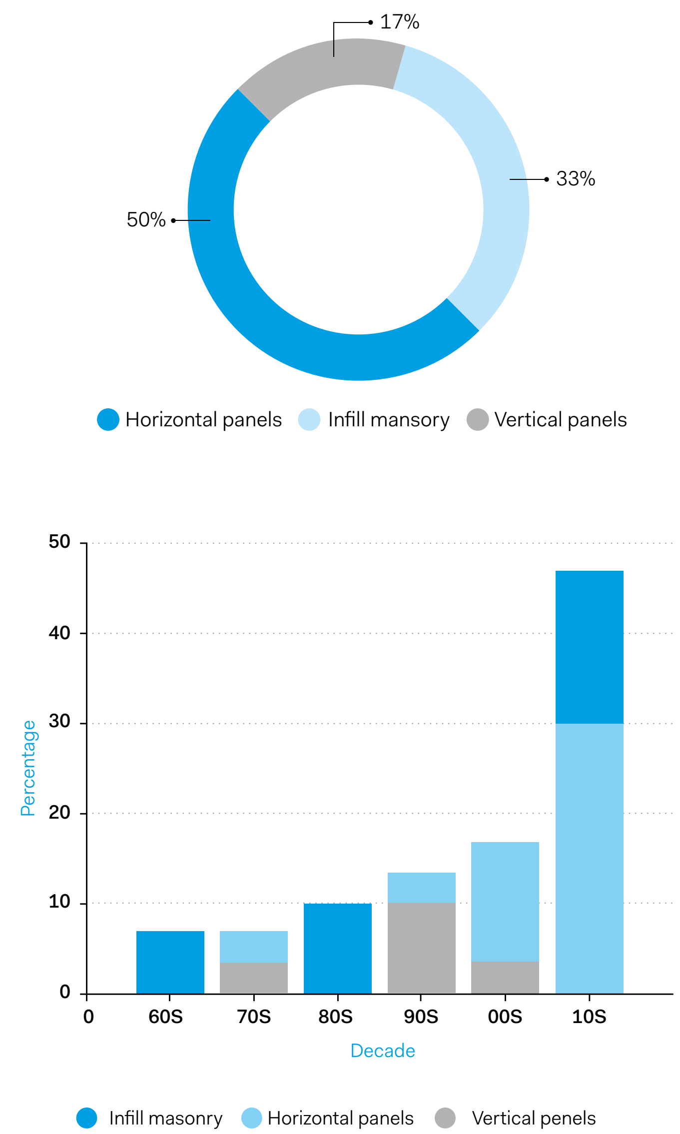

Figure 17 · Variation of type of cladding system by decade

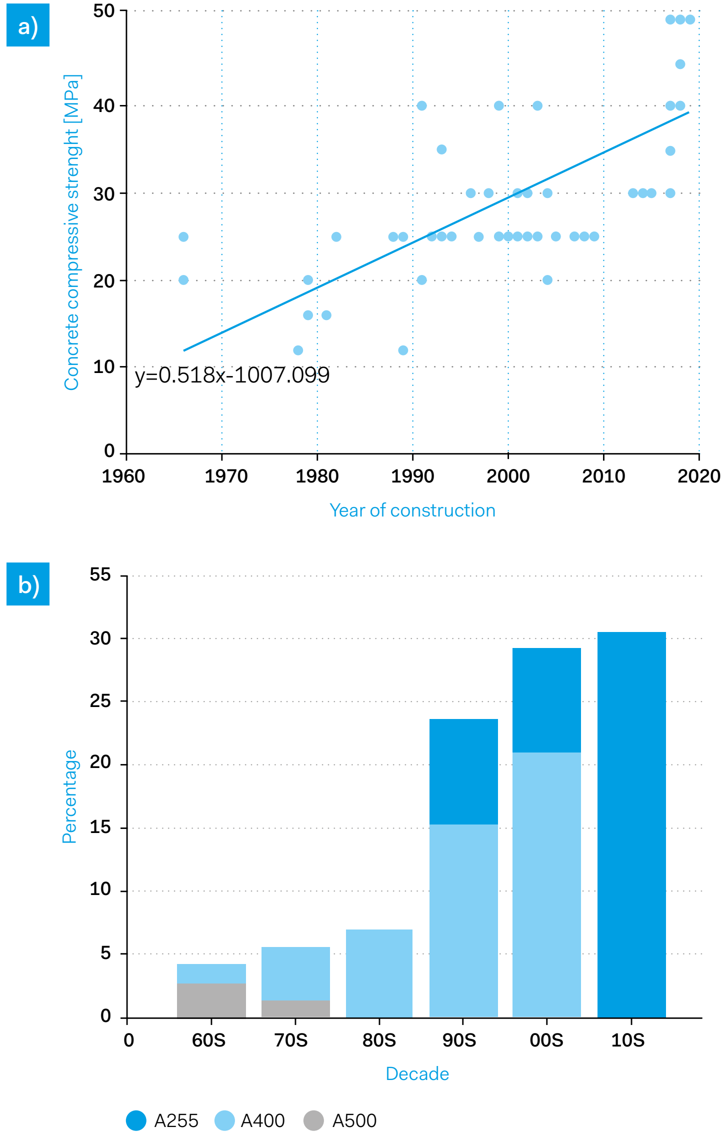

Figure 18 · a) Concrete and; b) Reinforcement strength evolution with the year of construction

Regarding the concrete class, Figure 18 a) shows a large dispersion of the concrete compressive strength (corresponding to the cylinder test) considered in the design process, despite the apparent important growth in the concrete strengths with the year of construction. Regarding the reinforcement, the number of classes is much lower than the ones found for concrete, and it is apparent that most of the RC members were built with A400 and A500 steel grades (Figure 18 b).

From a seismic point of view, the properties of the columns, namely the section dimensions and reinforcement ratios, assume relevancy stemming from their relative importance with respect to the beam members that, by virtue of their properties and structural arrangement, are expected to remain essentially undamaged. In this regard, it was observed that the columns are tendentially rectangular with mean values of 0.6 m (length) and 0.4 m (width), aligned along the longer span. Moreover, it was observed that the height-to-length ratio remains essentially unchanged with the year of construction and seismic hazard (Figure 19 a). Yet, it is evident that larger longitudinal (Figure 19 b) and transverse reinforcement ratios have been employed over time.

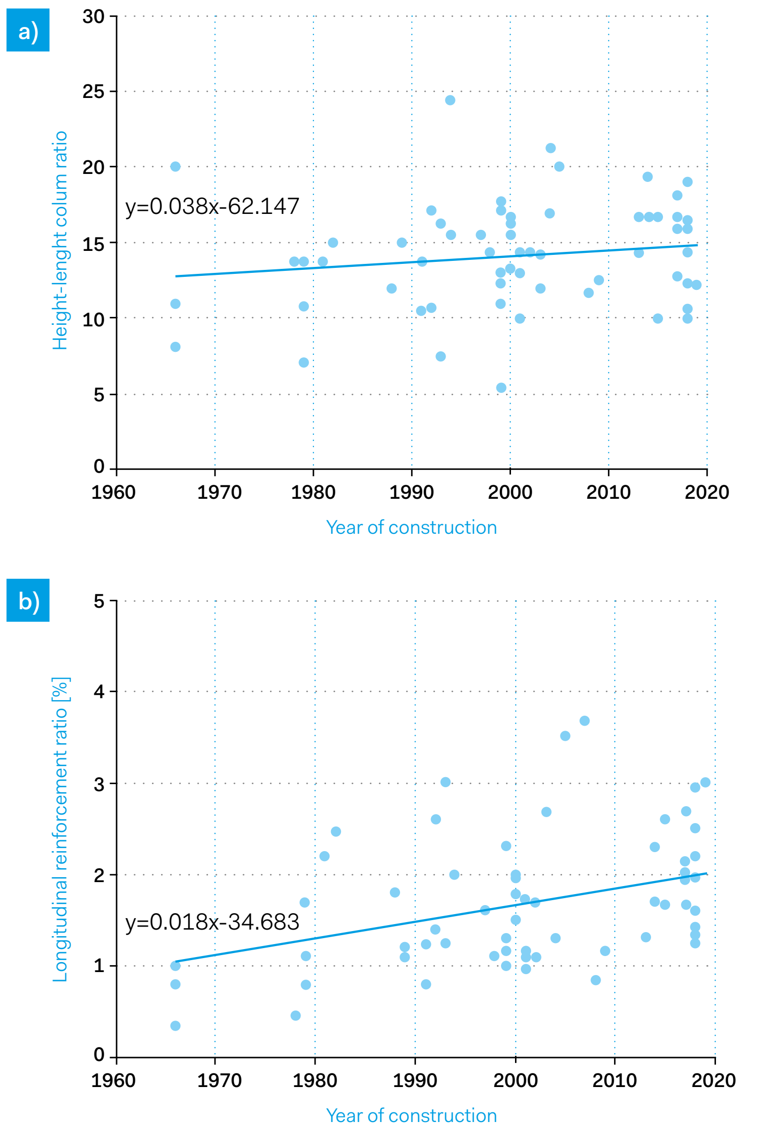

Figure 19 · a) Evolution of height-to-length column ratio and; b) Longitudinal reinforcement ratio with the year of construction

Past earthquakes showed that beam-to-column connections represent one of the main sources of damage in precast structures [2], [5], [6], [34]. Among the analyzed design projects, in nearly 60% of the cases, it was possible to access the details about the dowel connection. In the remaining cases, however, no reference to these elements was found, which may indicate that the beam-to-column connections could be ensured simply by friction in a reasonable number of buildings. Regarding the cases in which the dowels were detailed, the variability is significant both in terms of the number and diameter of the dowels (Figure 20) and appears to grow with the year of construction and be correlated with the beam span. On the other hand, the dowels' properties seem to be independent of the seismic hazard at the building site.

Table 1 presents an overview of the data collected from 73 PRC buildings together with the statistics derived for some of the properties.

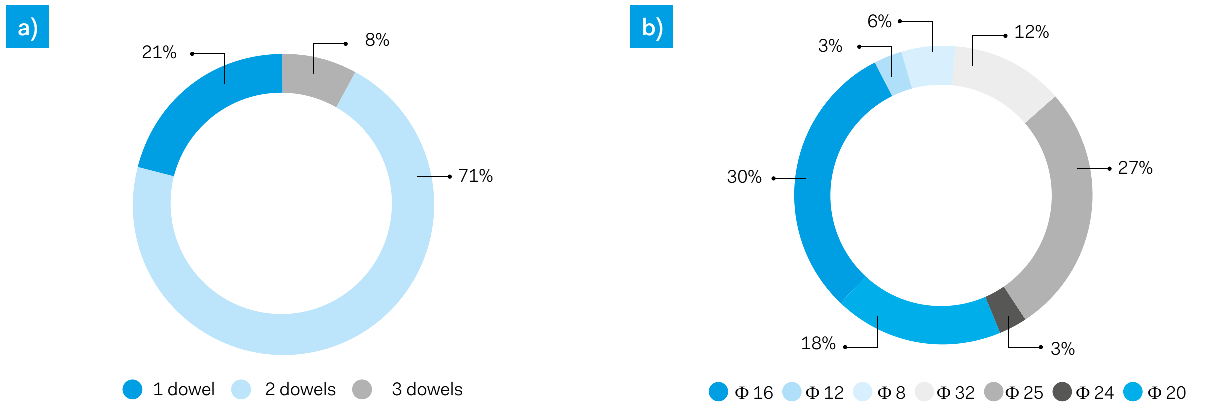

Figure 20 · Dowels in beam-to-column connections a) number and b) diameter

Table 1 · Summary of the distribution properties for the different parameters collected

Parameter	Mean	Median	Mode	COV [%]	Min	Max	Distribution	p-value [%]
Number of spans in longitudinal direction	2.3	2.0	1.0	94.1	1.0	11.0	Lognormal	0.0
Number of spans in transverse direction	8.2	8.0	8.0	58.3	1.0	29.0	Lognormal	7.6
Span length in longitudinal direction [m]	21.5	20.0	15.0	38.4	5.5	50.0	Lognormal	14.4
Span length in transverse direction [m]	7.6	6.5	5.0	32.9	4.2	12.5	Lognormal	0.0
Column height [m]	7.7	7.0	10.0	44.3	3.0	23.0	Lognormal	2.9
Column width [cm]	40.6	40.0	35.0	26.5	12.5	70.0	Lognormal	0.0
Column length [cm]	56.0	50.0	40.0	42.6	30.0	150.0	Lognormal	10.3
Column height-to-length ratio	18.1	18.8	20.0	21.9	6.9	28.9	Normal	5.1
Column length-to-width ratio	1.4	1.3	1.0	45.3	1.0	3.7	Lognormal	0.3
Longitudinal reinforcement ratio [%]	1.7	1.6	1.1	41.0	0.3	3.7	Lognormal	50.9
Transverse reinforcement ratio [%]	0.3	0.2	0.2	61.9	0.1	1.0	Lognormal	45.1
Corbel span [cm]	29.4	30.0	30.0	28.4	15.0	50.0	Lognormal	0.1
Concrete strength [MPa]	30.3	25.0	25.0	32.0	12	50	Lognormal	0.0

Seismic Precast ///

4. Experimental and numerical characterization of beam-to-column connections

4.1. Experimental characterization

The experimental studies are considered crucial to understand the behavior of structural elements, in particular, the beam-to-column connections.

The main objectives of this experimental research were to understand the influence of some parameters on the response of the precast beam-to-column connections, namely: i) friction between concrete faces; ii) friction between concrete and neoprene; iii) connection with a mechanic connector (dowels); iv) influence of the dowel positioned close to the edge of the column corbel: v) influence that different axial loads have on the overall response of the connection.

Despite the main aim of the study being the analysis of the connections under more controlled conditions, characterizing in a first stage the friction (with different surfaces, especially with concrete-neoprene) and the dowel contribution, it is important to recognize that, under strong seismic loads, the consideration of the rotation effects would allow representing the behavior of the connection in a more realistic manner. Yet, it would make it more difficult to characterize the different mechanisms involved properly. For this reason, the configuration adopted intends to reproduce a system with a pure shear response in the connection and thus be able to determine the friction coefficient for several surfaces

and levels of axial load with more precision. Nonetheless, it should be stressed that according to the work carried out by Zoubek *et al.* [35], under high seismic loads the capacity of the connection may be reduced in the order of 15-20% due to the development of relative rotations between the column and the beam.

The test setup was based on the review of the state-of-the-art of experimental works on precast beam-to-column connections. The detail of the specimens was established through the work of the typical properties of Portuguese precast industrial buildings presented by Rodrigues *et al.* [36], namely the column dimensions, corbel length and detailing, concrete compressive strength, longitudinal and transverse reinforcement grade, connections dowels, i.e., the number and the diameter, to represent a beam-to-column connection of a typical Portuguese industrial precast building, illustrated in Figure 21 in blue.

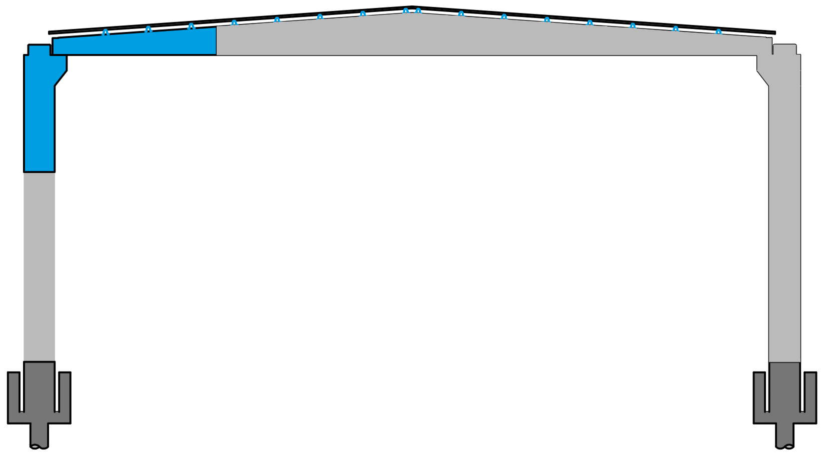

Figure 21 · **Schematic of the pretended beam-to-column connections to study (represented in red)**

A total of 12 tests were performed. The nomenclature adopted to each specimen was “SPC_xx_yy” where ‘xx’ stands for the interface type, namely i0 for the concrete interface (Figure 22a), i1 for one neoprene pad layer, i2 for two neoprene pads layers (Figure 22b), c1 for specimens with 2 dowels of 16 mm of diameter and placed 13 cm from the internal face of the column (Figure 22c) and c2 for specimens with 2 dowels of 16 mm of diameter and placed 6 cm from the internal face of the column (Figure 22d). The ‘yy’ stands for the axial load applied.

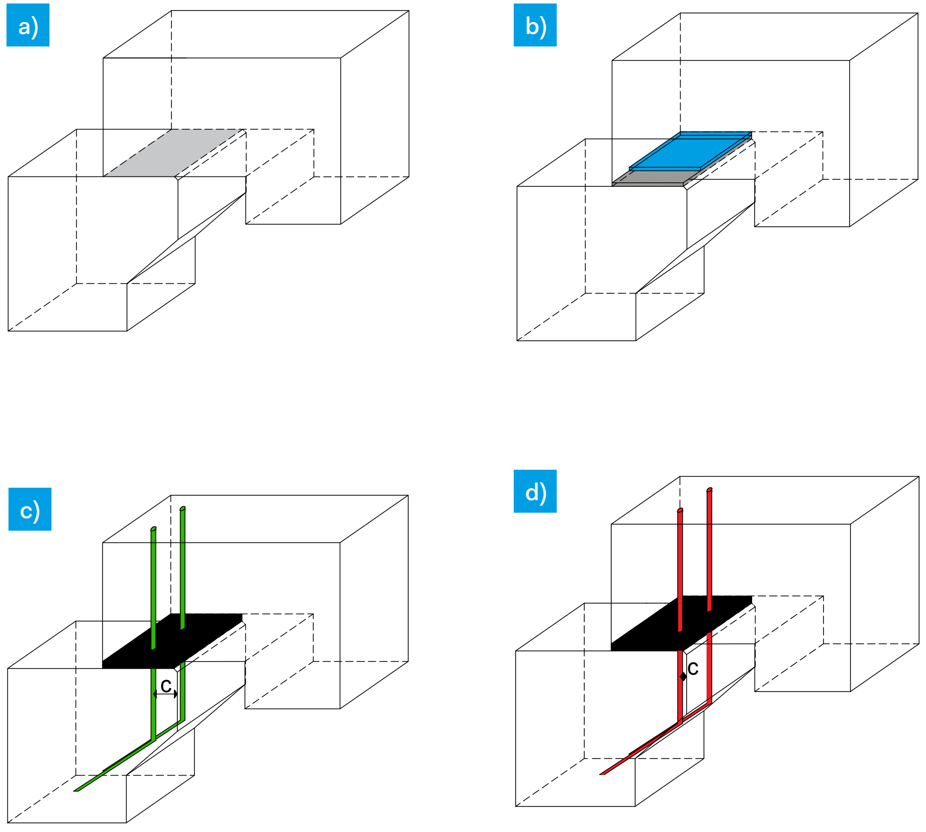

a) Friction between concrete faces – i0

b) Friction between concrete and neoprene pads: 1 neoprene pad (grey) – i1 – or 2 neoprene pads (grey and blue) – i2

c) Dowel influence: dowels centered (green) – c1

d) Dowel influence: dowels placed on the face (red) – c2

Figure 22 · **Scheme of the parameters under study**

Figure 23 shows the experimental setup adopted. Two hydraulic actuators were used: one vertical to apply the axial load with a maximum capacity of 200 kN and a +/−100 mm stroke, and the other actuator was placed horizontally to apply the lateral load with a maximum capacity of 200 kN and a +/- 150 mm stroke. The actuator was positioned to be centered horizontally with the connection. The same concern was taken with the positioning of the vertical actuator, which was placed in the middle length of the support (15 cm from the end of the beam). The column was fixed to the reaction frame to simulate a fixed column at the base.

The horizontal actuator applied displacement-controlled lateral cyclic loading according to the displacement history at a constant velocity of 0.2mm/s. The displacement history was defined to capture the stiffness and strength degradation through the cycle repetition. Each displacement level was repeated three times: from 0 to 5 mm with a difference of 1 mm and from 5 to 45 mm with a 5 mm difference between the incremental cycles.

The loading of the horizontal actuator was monitored through a load cell, and the applied horizontal displacement was measured using an internal and an external displacement transducer.

The axial load considered in the experimental test varies from 50 to 150 kN at the connection level, representing the beam's self-weight and the additional dead load from the self-weight of the roof structures and finishing's.

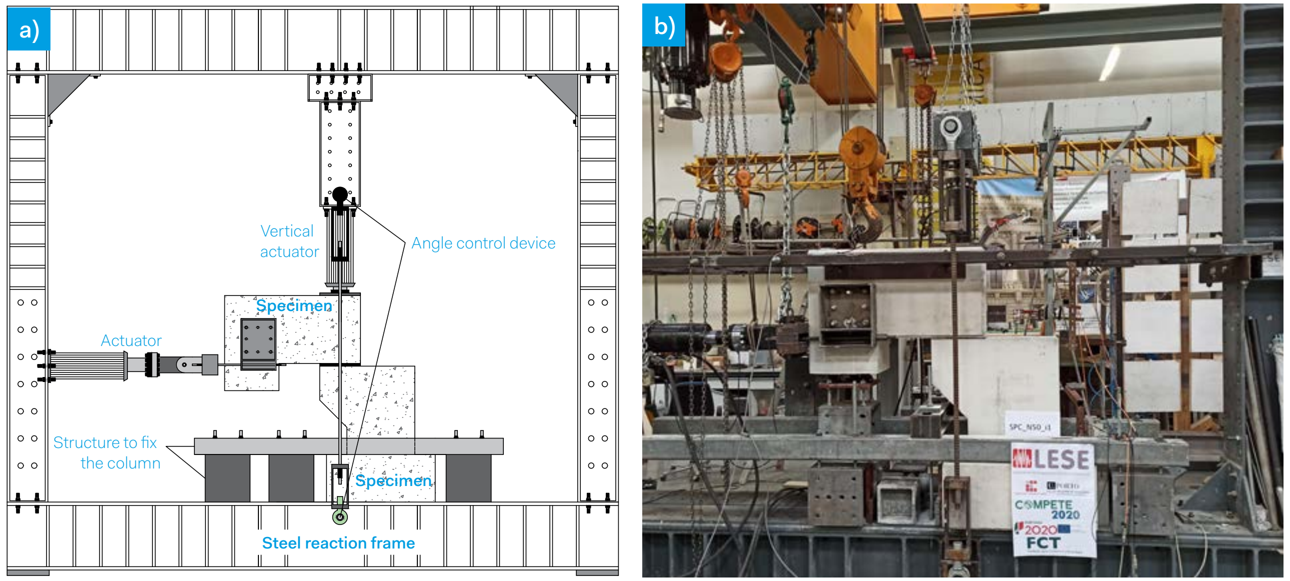

a) Schematic layout
b) General view

Figure 23 · **Testing setup**

The main experimental results obtained in the testing campaign are herein presented, with the discussion of the force-displacement hysteretic curves results, the most representative damages, and other aspects considered important to discuss. The results were grouped according to their interface type.

Seismic Precast ///

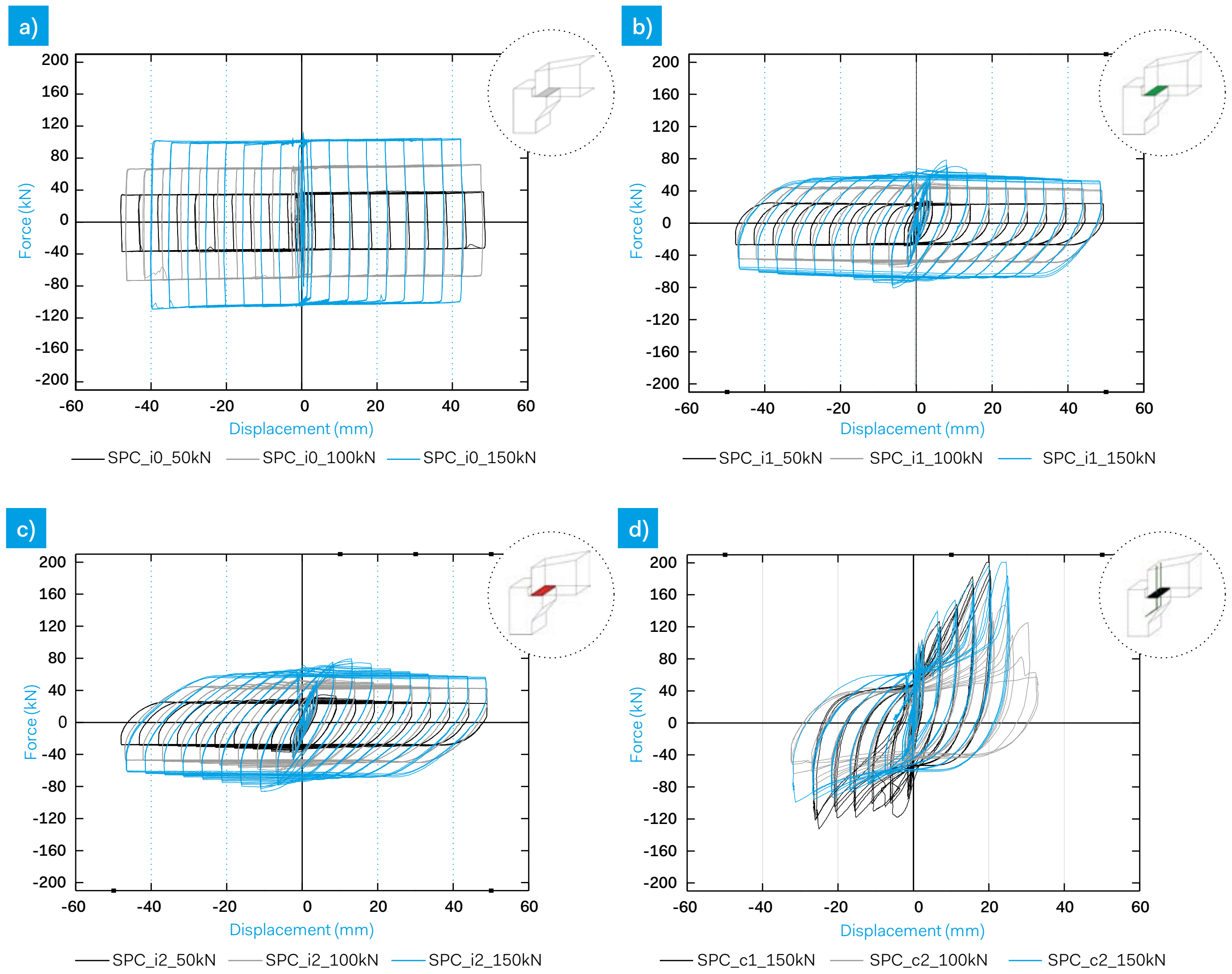

a) Concrete-concrete interface (i0)
b) Concrete-neoprene interface (i1)
c) Concrete-neoprene interface (i2)
d) Dowel interface (c1 &c2)

Figure 24 · **Force-displacement hysteretic curves**

Regarding the concrete-concrete interface results (Figure 24a), the large hysteretic loops in unloading stages, are specific to concrete interface connections, as noticed by Sousa *et al*. [37]. Once the force applied in this type of connection is equal to friction force (corresponding to the static friction coefficient), there is no need to increase the beam's force to slide over the column. The curves presented in Figure 24a), show that the increment of the applied axial load leads to an increase of the lateral force. In the case of an axial load level of 50kN, the maximum lateral force is around 39 kN, which is 53% and 62% lower than what was obtained in the testing of specimens SPC_i0_100kN and SPC_i0_150kN, respectively. According to the results obtained, a friction coefficient of around 0.75 was obtained, which is in line with the one mentioned in [7], where the authors referred that the friction coefficient between concrete faces varies between 0.5 and 1.2, depending on surface roughness and normal stress.

Moving on to the analyses of test specimens with one layer of neoprene pad (Figure 24b), an increase of the axial load to the double and triple, corresponded to an increase of about 48% and 64% of the lateral force for SPC_i1_100kN and SPC_i1_150kN compared with SPC_i1_50kN. Comparing the test specimens' hysteretic curves with one (Figure 24b) and two layers of neoprene pads (Figure 24c), the first important conclusion is that using a higher thickness does not affect the strength of the connection. The most significant difference that can be observed when comparing the test specimens i1 with i2 is the flexibility of the connection, which can be noticed through the beginning of the reloading stages where the curve has a higher slope which is translated by the lower stiffness of the neoprene pad, leading to smaller dissipated energy. Moreover, it is essential to mention that the neoprene stiffness depends on the shear modulus of the neoprene, the contact area between the concrete and the neoprene pad, and finally, the neoprene pad's thickness. Thus, the greater the neoprene thickness, the less stiffness of the neoprene pad.

Finally, regarding the results of the hysteretic curves of specimens with dowels (Figure 24d) the first general conclusion from the three tests is that the connection response is not symmetric in terms of lateral strength in all the tests. The maximum strength in the pull direction was practically half of the one in the push direction.

For interface c2 it can be noticed a decrease of 50% in SPC_c2_100 kN and 51% in SPC_c2_150 kN. In the c1 interface case (SPC_c1_150kN), the push and pull direction difference is also significant. However, it is lower than in the previous cases with a decrease of 34% of the force applied. These results are directly related to the dowels' covering thickness in the pull direction. For this reason, in the case of the specimen with the most centered dowels (c1), the strength is more significant, as it presents a greater coverage of the dowels (not so prone to spalling). On the other hand, the test specimens with the dowels closer to the column face (c2) showed a more significant difference between the load application directions, showing a higher vulnerability in the pull direction with the concrete spalling occurring earlier when compared with the other specimens.

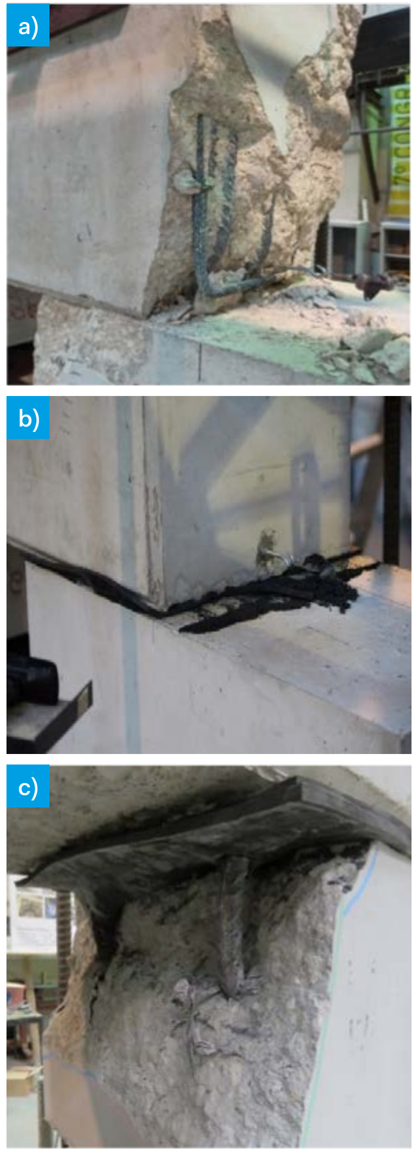

a) SPC_i0_150kN
b) SPC_i1_100kN
c) SPC_c2_100kN

Figure 25 · **Damages observed in the specimens**

Regarding the damages observed, the specimens without neoprene or dowels (i.e. i0) were the ones that showed the most significant damage in general. At the end of these tests, the specimens were quite damaged. This type of interface test was the only one that showed the damage at the level of the beams, as illustrated in the Figure 25a. The damage occurs when the cohesion between the microscopic particles is exceeded.

The damage of the specimens with neoprene between the concrete interfaces (i.e. i1 & i2) is shown in Figure 25b. These experimental tests were the ones that led to light damage at the level of the columns, showing no visible damage at the beams. As Zhang et. al [38] mentioned, even a thin rubber (neoprene) pad added to the interface can modify the mechanical response of two concrete structures by interacting mechanically, changing friction and contact condition.

Regarding the damages observed in the specimens with dowels (i.e. c1 & c2), the damage was concentrated only on the columns, namely on the corbel level (Figure 25c), with no damage at the beam level. All specimens presented cracks developed from the dowel's location due to local stresses. Despite this, these cracks developed at different times of the tests. Regarding the specimen SPC_c1_150kN the first crack appeared in the 10 mm cycle at the level of the dowels and the total detachment of the concrete occurred in the 30 mm cycle. The specimen SPC_c2_100kN developed the first crack in the 2 mm cycle and showed total detachment of the concrete in the 10 mm cycle. Finally, specimen SPC_c2_150kN presented the first crack in the 3 mm cycle and spalling of the corbel concrete in the 10 mm cycle.

In short, dowel connections showed significant damage but showed greater strength and resistant capacity due to the considerable contribution of dowels.

4.2. Numerical modelling

The proposed model presents an efficient macro-element capable of accurately describing the main mechanisms identified in conventional beam-to-column PRC connections, namely the friction, dowel behavior, and the neoprene components' contribution.

The numerical simulation of connection systems on efficient software packages has been addressed in the past by several authors, [21], [34], [39], [40]–[43]. However, these models are simplistic, failing to describe the different mechanisms independently and, therefore, are difficult to apply to generic connection solutions, or are too complex, computationally demanding, and unsuitable for common engineering applications or seismic risk analysis. This modeling approach can be easily defined in conventional beam-to-column elements numerical analysis software packages. Figure 26 illustrates the idealization adopted to simulate the different resisting systems: the friction between the different elements, the steel dowels and the neoprene pad. A typical configuration of beam-to-column connections is shown on the left-hand side in existing PRC buildings, while on the right-hand side is a mirrored scheme of the idealized numerical model.

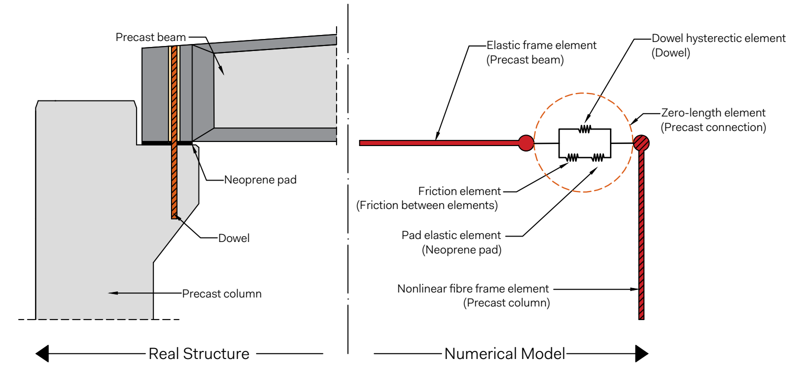

Figure 26 · **Beam-to-column connections in conventional PRC buildings: common configuration (left) and numerical arrangement adopted (right)**

Seismic Precast ///

The accuracy of the proposed numerical model was assessed against the results of four experimental tests described in detail by Psycharis and Mouzakis [44], considered as the benchmark in the scope of the present study. To access the accuracy of the numerical model, each experimental test was simulated considering the set of parameters previously defined. Figure 27 shows the comparison between the experimental results and the numerical models.

The comparison of the results demonstrated the ability of the model to estimate the maximum strength of the connections considering the two main failure mechanisms (dowel rupture and concrete spalling) and the strength degradation effects.

The study showed the ability of the model to simulate generic beam-to-column PRC connections featuring a large diversity of properties. Moreover, it highlights the important contribution of the dowels for the total lateral strength and the need to incorporate the friction component to obtain a reliable estimate of the energy dissipation of the system.

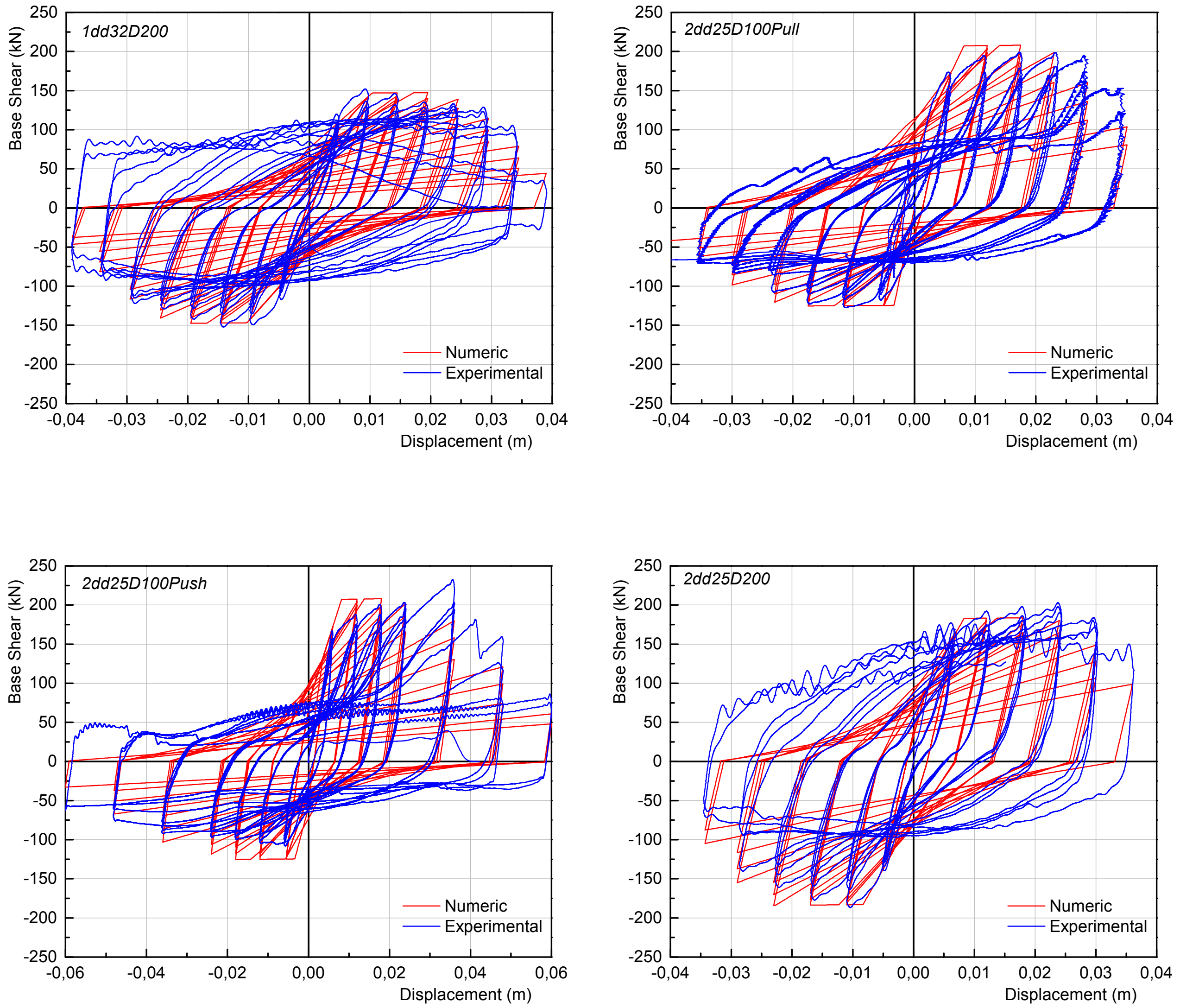

Figure 27 · **Comparison between experimental response and numerical predictions of the models tested**

5.
Influence of beam-to-column connections in the seismic performance of PRC buildings

The main objective of this study is to understand the influence of the beam-to-column connections (dowels, neoprene pads and friction between the elements) in the seismic response of PRC structures. Making use of the previously presented macro-element to accurately describe the main mechanisms identified in conventional beam-to-column connections, the results obtained provide indications on suitable modeling strategies and numerical assumptions for the design and assessment of existing PRC.

5.1. Description of the case study

The PRC building under study represents an existing industrial framed structure (Figure 28) constituted by one floor with an area of 180 × 175 m² and a height of 12 m. The structure has 5 spans in the X direction (Figure 29) with 35 m of length each and 15 spans in the Y direction with 12 m of length each. The columns of the structure have a height of 12 m (the height of the building) and a rectangular section of 0,70 × 0,50 m² (Figure 30) with a 40 mm cover. The concrete used was C40/50 and the steel the S500 NR-SD. The beams are prestressed with an "I" variable section, with a length of 36 m and a 30 mm cover. The columns are assumed fixed to the foundation.

Figure 28 · **3D overview of the building under study**

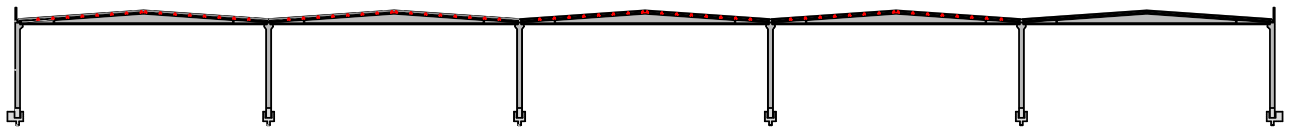

Figure 29 · **Principal direction (X) of the framed structure**

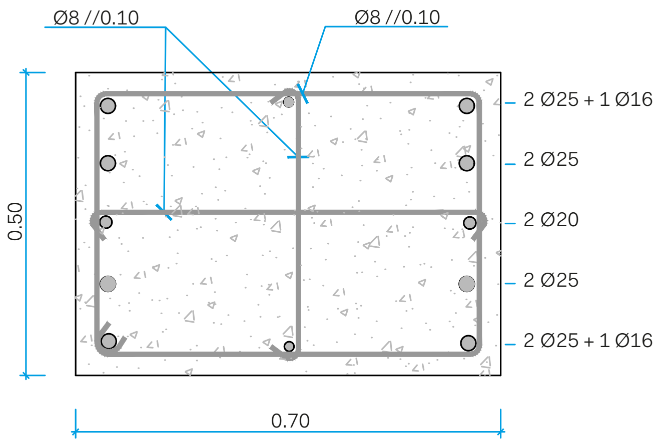

Figure 30 · **Column section**

In Europe, the most common type of beam-to-column connection in PRC industrial buildings is the dowel connection [45]. In this system, the beam is mechanically connected to the column through vertical steel dowels. These dowels, usually one or two, protruding from the column's corbel (Figure 31) fit into sleeves left in the edge of the beams, which are later filled with a proper grout. In several cases, a steel or neoprene pad is placed between the column and the beam. These connections do not restrain the rotations between both members, while the transfer of horizontal forces between the beam and column is essentially ensured by friction and dowels (if present).

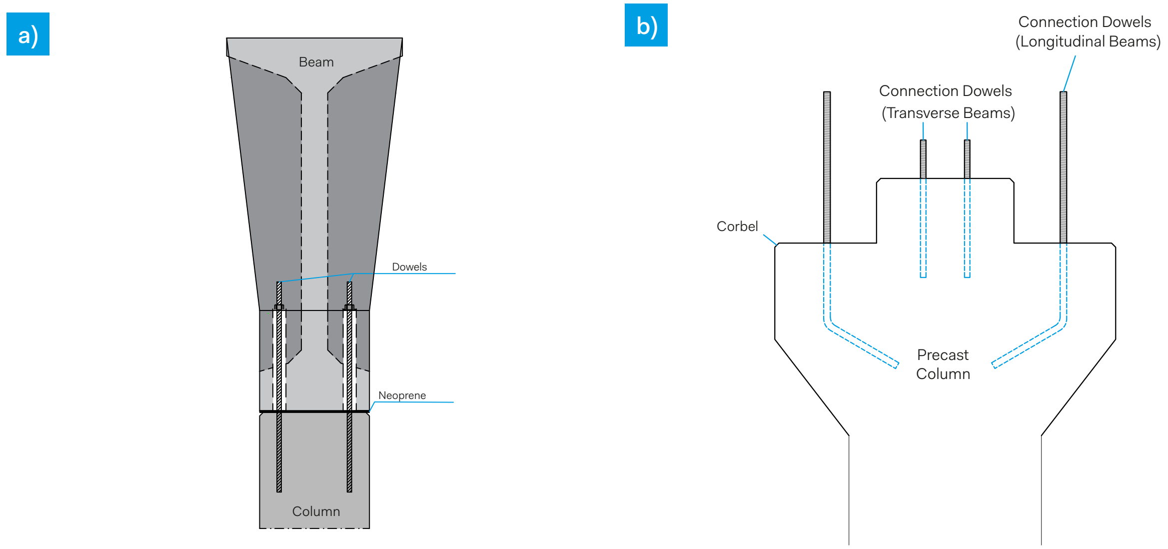

a) Beam-to-column connection
b) Central column detailing

Figure 31 · **Scheme of conventional European beam-to-column dowel connection**

5.2. Static loads and seismic action

For the numerical analyses, constant vertical loads distributed on beams were considered to simulate the dead load of the roof and PRC elements self-weight, and the corresponding quasi-permanent value of the live loads, giving a total value of 0.65 kN/m². The mass of the structure was also assumed to be distributed at beam levels. The models were subjected to incremental dynamic analysis (IDA). A total of ten ground motion records were selected from real seismic events according to the Araújo *et al.* [46] method. The average of the earthquake records fit the Eurocode 8 target spectrum for Type 1, for Lisbon, and soil type A, as illustrated in Figure 32.

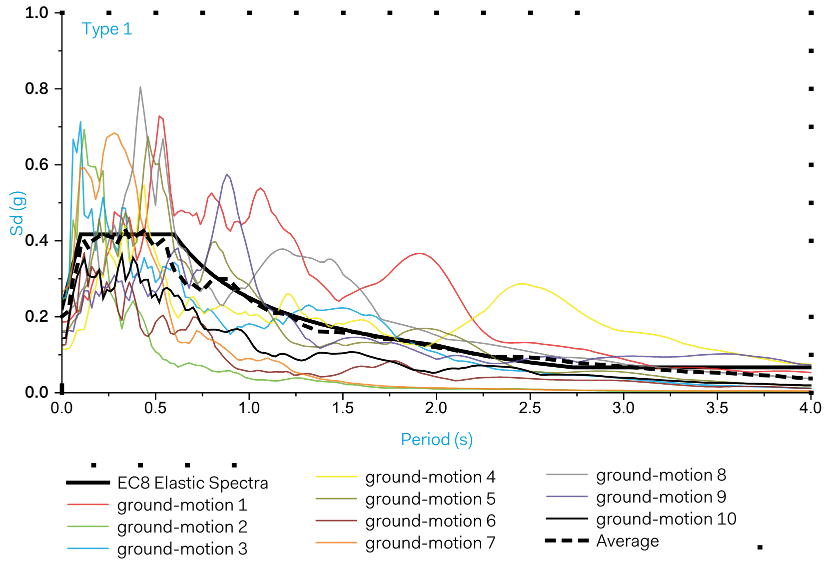

Figure 32 · **Elastic spectrum of the ground motions selected (Type 1)**

5.3. Sensitivity parameters

A parametric study was developed to understand the seismic performance of the structure. After, several cases were considered to better understand the impact that certain parameters have on the response of the building being studied. The parameters considered are focused on the response of the beam-to-column connections, namely regarding the relative importance of the contribution of the dowels, neoprene and friction. Each case was named according to the properties considered in the model, for example, the case DFNC corresponds to a Dowel, Friction and Neoprene

Connection considered in the model, in the same way, the case DC corresponds to a Dowel Connection and the case FNC corresponds to a Friction and Neoprene Connection considered in the model. The model PC corresponds to Pinned Connections considered in the model. The properties adopted in the different models are listed in Table 2.

Table 2 · **List of the properties adopted in the different models**

	Number/Diameter of Dowels [mm]		Friction	Neoprene Pad [mm]
	X Dir.	Y Dir.		
PC	Pinned connection			
DFNC	2 Ø24	2 Ø20	Yes	20
DC	2 Ø24	2 Ø20	NC	NC
FNC	NC	NC	Yes	20

5.4. Results

5.4.1. DFNC connection and pinned connection

In the present section, the DFNC model is compared with the PC model to find the difference between considering a model with a connection with a dowel, friction, and neoprene and a model with pinned connections, usually considered in the common design practice. In Figure 33 the drifts and seismic coefficients for the DFNC and PC models are represented. The differences between the DFNC and PC models are very low, indicating that, in cases where the connection is adequately designed, i.e., the connection is capacity protected with respect to the level of forces expected in the adjacent columns, the seismic behavior of the building can be modeled with acceptable accuracy using simple pinned connection models.

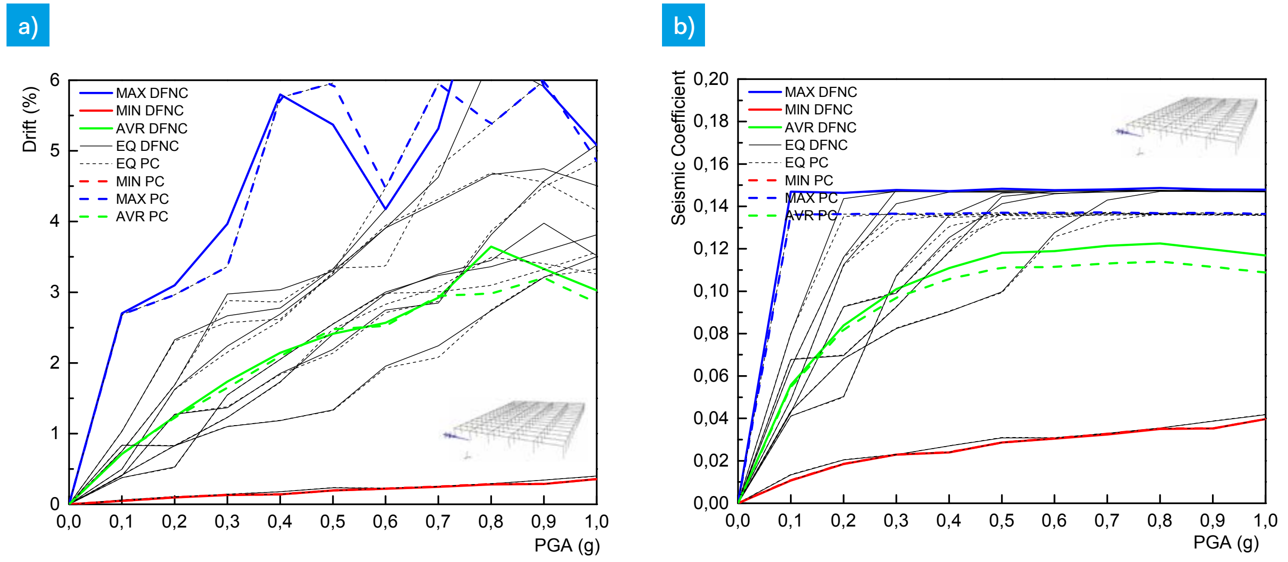

a) Drift comparison
b) Seismic coefficient comparison

Figure 33 · **Model 3D with pinned and DFNC connections for earthquake type 1 in X direction**

5.4.2. Effect of neoprene and friction

This section discusses the comparisons of the drift and seismic coefficient of the 3D models with DC and DFNC connections, to evaluate the effect of the connection only with the dowel and the connection considering the dowel, friction and neoprene. For the building understudy, this effect does not seem to play a significant role. Figure 34 shows that the influence of friction and neoprene is low in terms of drift and seismic coefficient of the structure. In fact, previous studies [37] pointed to a contribution of the friction and neoprene of around 25% of the global connection response. Such values are not observed in this case because the columns are significantly more flexible than connections with dowels, even if the friction and neoprene are neglected and, therefore, the horizontal response of the building is governed by the flexibility of the columns.

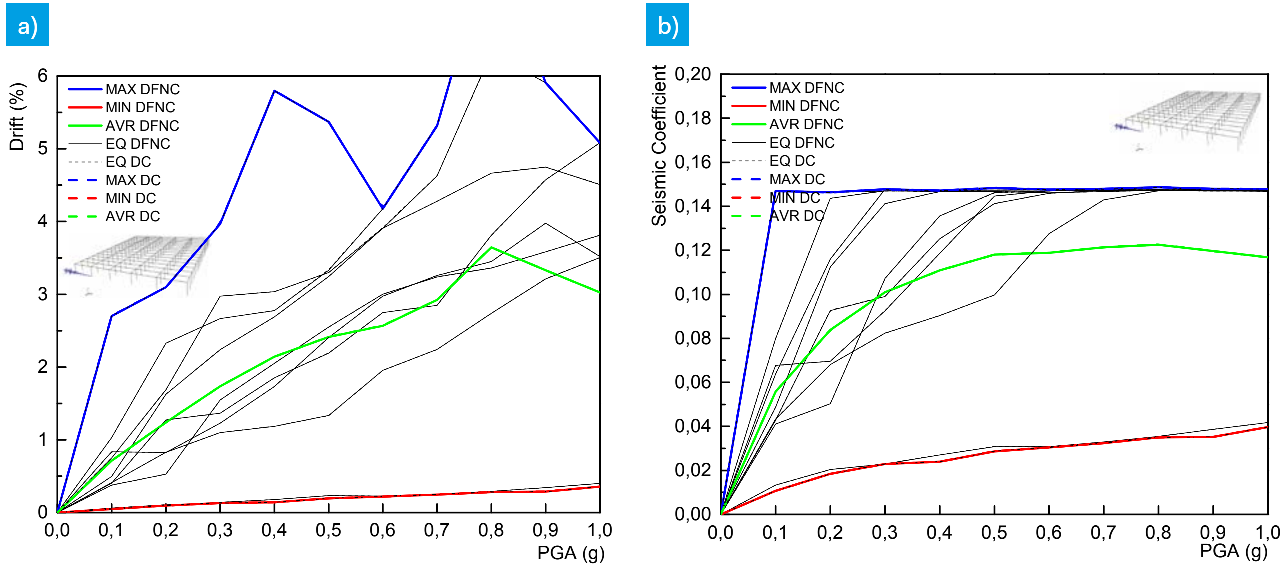

a) Drift comparison
b) Seismic coefficient comparison

Figure 34 · **Model 3D with DC and DFNC connections for earthquake type 1 in X direction**

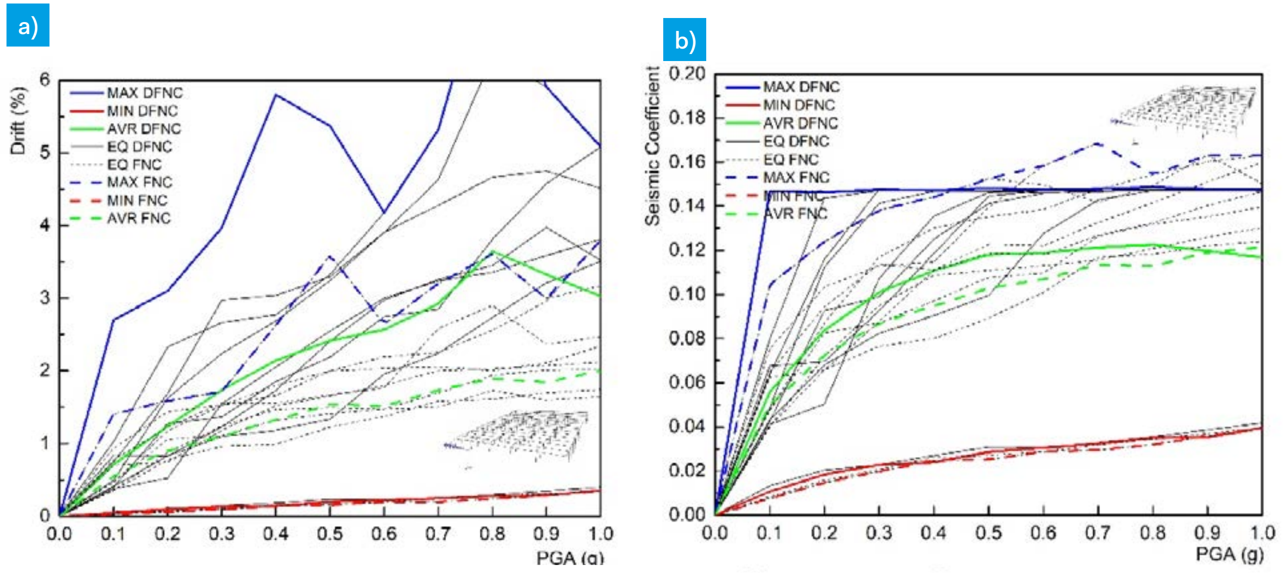

a) Drift comparison
b) Seismic coefficient comparison

Figure 35 · **Model 3D with DFNC and FNC connections and for earthquake type 1 in X direction**

5.4.3. Effect of the dowels

In this section it is presented the comparative analysis of the 3D models with FNC and DFNC connections. Figure 35 shows a significant difference between considering FNC and DFNC connections, which highlights the importance of the dowels in the overall seismic behavior of the structure. For the same level of PGA, the columns in the model without dowel present a lower drift demand when compared with the model with dowels (Figure 35 a). On the other hand, DFNC connections have higher seismic coefficients when compared with the FNC connections (Figure 35 b) due to the connection sliding that in the models without dowels are much higher than those with dowels (Figure 36). The previous observations show that the deformations are essentially concentrated in the connection in the model without dowel. Assuming a limit for connection maximum sliding of 350 mm based on typical geometric properties of the beams' support [25], it is possible to see that, for PGA higher than 0.45 g, the connection fails for the average of the analyses.

The results observed are in line with the damage observed after past seismic events such as the Emilia earthquake of 20th and 29th of May 2012. In fact, the damage observed in the connections occurs essentially in buildings without dowels. In these cases, the horizontal strength at the connection level is ensured essentially by friction, and hence its capacity to sustain horizontal loads is severely compromised. This observation highlights the need to consider detailed connections models, capable of simulating the different strength mechanisms at the connections, to conduct a reliable seismic assessment of existing buildings, especially those built without considering steel dowels.

Seismic Precast ///

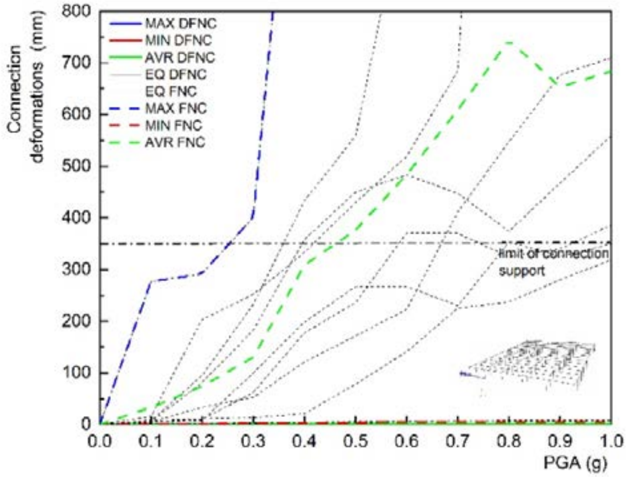

Figure 36 · **Connection sliding in model 3D (12 m) with DFNC and FNC**

5.5. Main conclusions

The work discusses a parametric study carried out through a series of nonlinear dynamic analyses on 3D PRC building models aiming to evaluate the contribution of the different beam-to-column connection mechanisms in the seismic behavior of the building. For this purpose, the properties of the numerical model developed were defined to mimic common industrial buildings with this typology. For this reason, it is believed that the discussion of the results obtained in this study is not necessarily limited to the case study considered. It is possible to extract conclusions that are valid for the generality of this typology of building.

PRC buildings are generally flexible structures when compared with conventional RC buildings. For this reason, these buildings tend to be more sensitive to ground motion from long epicentral distances, which tend to present more significant spectral accelerations for longer periods of vibration (commonly designated as seismic action Type I, according with EC8).

Regarding the seismic behavior of beam-to-column connections, from a general point of view, the results showed the importance of these elements to the seismic behavior of the entire structure. In the presence of adequately designed dowels, small deformations are expected at the connections level and, therefore, the response of the structures is controlled by the properties of the columns. For these cases, the consideration of a simple pinned connection appears to be an efficient and accurate numerical approach.

On the other hand, in the absence of dowels, or in cases where these are not properly designed, a concentration of damage is expected to occur at the connection level, whilst the columns remain essentially undeformed, which is in line with the damage observed in field observations after recent earthquakes.

For intermediate cases, i.e., beam-to-column connections featuring conventional diameter dowels, the explicit consideration of the connection properties through a reliable numerical model is advocated in order to estimate the actual capacity of the connection, especially in terms of deformation, in order to avoid local damage or even the collapse of the beams.

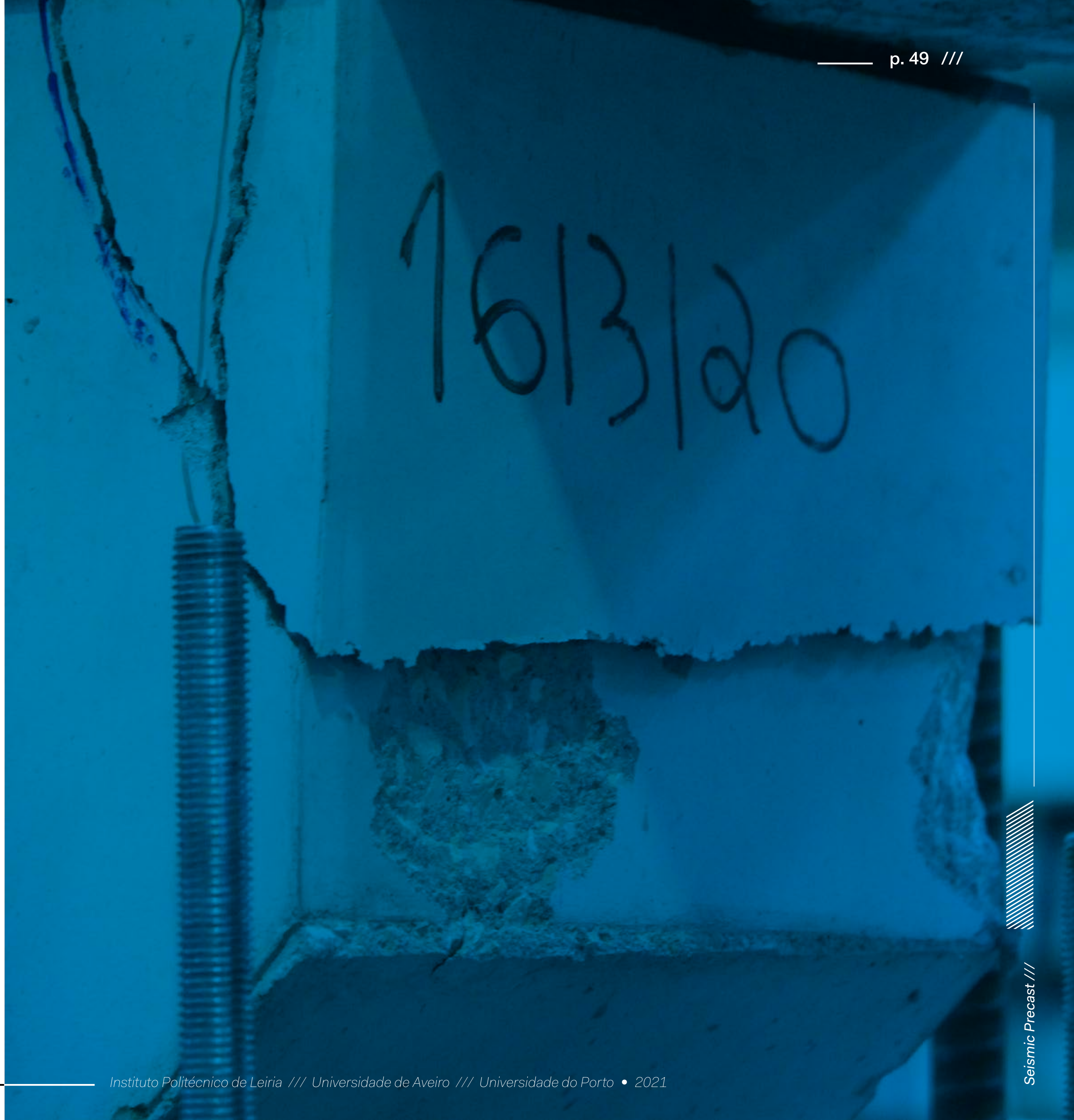

6. Seismic assessment of precast buildings according to EC8-3

6.1. Characterization of the case-study building

The existing PRC building considered to perform the seismic assessment, following the prescriptions of the Eurocode 8 – part 3, was collected from the database, whose results were presented in Rodrigues *et al*. [25], and briefly presented in Chapter 3. Given the lack of specific codes addressing the design of PRC buildings in Portugal, it was decided to define three sub-classes based on the year of construction, as an important fraction of the mechanical and geometric properties depend on the year of construction. The sub-classes were defined as 'Pre code', 'Moderate code' and 'Post code'. The 'Pre code' buildings were defined as those built from 1960 to 1980, the 'Moderate code' from 1980 to 2000, and the 'Post code' from 2000 to 2020. One building from 'Moderate code' was analyzed corresponding to seismic zone 1.3 (type 1).

6.2. Geometric and mechanical characterization of the building

The global configuration of the building analyzed is presented in Figure 37 while the main geometric and material characteristics are summarized in Table 3 and Table 4, respectively.

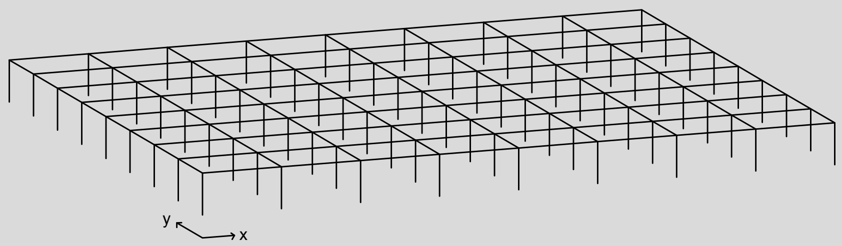

Figure 37 · **Model of the building B3_ModC**

Regarding the geometric characteristics (Table 3), the column slenderness ratio was calculated according to the expression described below and recommended in EC2 [48]:

$$\lambda = \frac{l_0}{i} \quad (1)$$

where l_0 is the effective length and i is the radius of gyration of the uncracked concrete section. The slenderness was calculated for both directions and the values are shown in the Table 3.

Table 3 · Geometric characteristics of the buildings in studying

Structure ID	Number of spans		Span length		Height [m]	Columns Slenderness	
	x	y	x [m]	y [m]		x	y
B3_ModC	8	8	17.0	6.0	9.0	69	89

Table 4 · Material and reinforcement detailing characterization

Building ID	Concretefcm [MPa]	Steel fym [MPa]	Column b×h [m]	% Steel		Dowel Ø [mm]
				Longitudinal	Transversal	
B3_ModC	33	440	0.45×0.35	1.60	0.17	2Ø16

The properties of the buildings selected reflect the evolution in terms of geometry and material observed with the year of the design project (Table 4). For instance, in the 'Moderate Code' building the connection is made by means of a mechanical element – the dowel – combined with the friction component.

6.3. Numerical modelling

The structural behavior of the PRC building was simulated along with the two main directions with a 3D model using the structural analysis software Opensees [49]. In these models, the columns were simulated using force-based nonlinearBeamColumn elements with distributed inelasticity with 5 integration points in each element, whilst the beams, which are expected to remain undamaged, were modeled with linear elastic elements. In terms of materials, for the concrete, it was used the Concrete02 model, whereas the columns' longitudinal reinforcement was simulated considered the Steel02 model, based on the Giuffre-Menegotto-Pinto [50] material model. Regarding the beam-to-column connections, its behavior was simulated through a macro-element proposed by Sousa et al. [37], which can precisely describe the main mechanisms identified in conventional beam-to-column PRC connections, namely friction between the different elements, steel dowels and the neoprene pad.

6.4. Nonlinear static analysis

The assessment of the building was firstly carried out through nonlinear static (pushover) analyses. These analyses were carried out along the two main directions of the buildings adopting a distribution of incremental horizontal forces proportional to the shape of the fundamental modes and a uniform distribution proportional to the mass, according to the Eurocode 8 recommendations. For both cases, it was also considered inclusion of the effects of the accidental eccentricity, through the movement of the mass by 5% of the building's length perpendicularly to the direction of the acting seismic action, in order to account for possible variations in the distribution of masses in the structures. Additionally, the normative resistance for the flexural and shear mechanisms was calculated, along with the appliance of the N2 method, as defined in the Eurocode 8 [30].

The determination of the target displacement associated with the seismic hazard at the building location was based on the procedure presented in Annex B of Eurocode 8 – Part 1 [30], adopting an iterative procedure for improved accuracy. This approach follows the N2 method proposed by Fajfar [51] and enables the determination of the building's seismic demand based on the elastic (5% damped) response spectrum. Hereafter, the responses of the elements at the global target displacement are compared against the elements' capacity to assess their expected seismic performance.

6.5. N2 method procedure

To perform the assessment of the existing PRC industrial buildings the N2 method was used as stated before. This subsection will present the method used to estimate the maximum deformation (displacement) that the structure in the study can perform. This displacement reflects the structural limit state of the building and can be applied in reverse as a tool to implement the direct displacement-based design (DDBD).

The input data are the structure in study (masses), the pushover curve and the elastic spectrum of accelerations (Figure 38). To demonstrate the methodology carried out by the N2 method, the steps to building B3_ModC to direction x will be presented as an example.

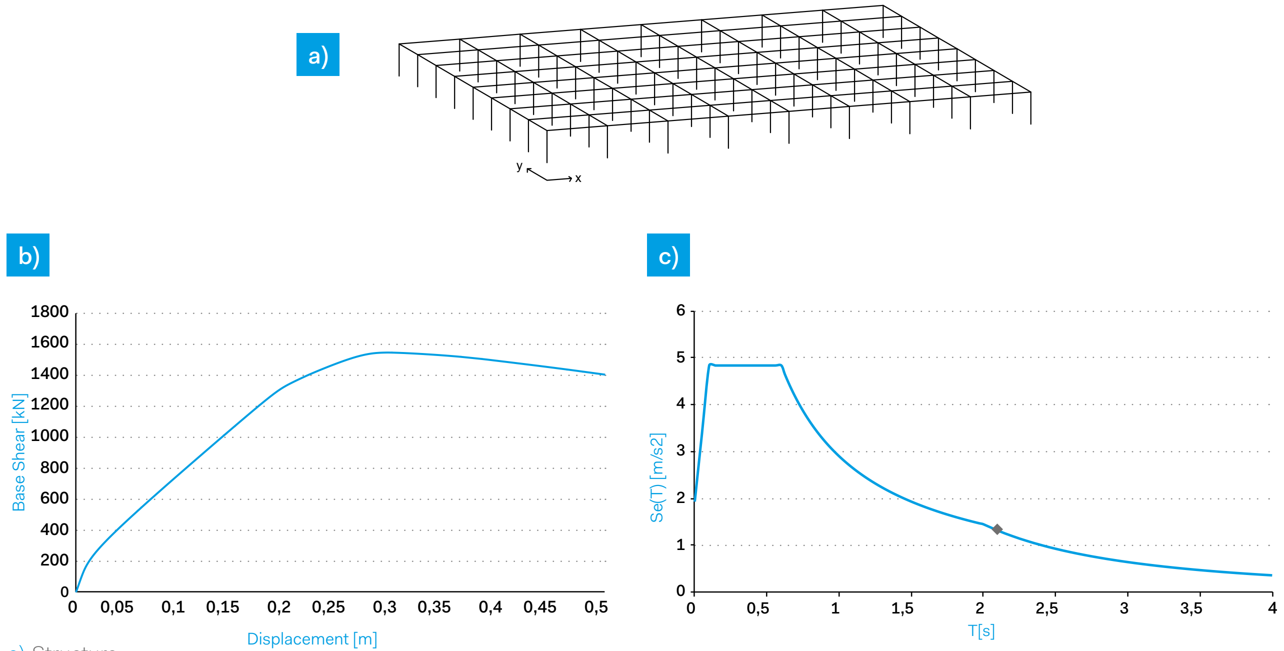

a) Structure
b) Pushover curve
c) Elastic spectrum

Figure 38 · **Input data to N2 method**

Once industrial buildings are mostly single-storey, converting to a degree of freedom structure is simpler. The expression (2) relates normalized lateral forces ($\overline{F}_i$) and normalized displacements (Φ_i), where the m_i is the mass of each floor. To transform the structure into an equivalent system of a single degree of freedom (SDOF) expressions (3) to (6) are used. More details can be found in Annex B of Eurocode 8 – Part 1 [30].

$$\overline{F}_i = m_i \Phi_i \quad (2)$$

$$m^* = \sum m_i \Phi_i = \sum \overline{F}_i \quad (3)$$

$$\Gamma = \frac{m^*}{\sum m^i \Phi_i^2} = \frac{\sum \overline{F}_i}{\sum \left(\frac{\overline{F}_i^2}{m_i} \right)} \quad (4)$$

$$F^* = \frac{F_b}{\Gamma} \quad (5)$$

$$d^* = \frac{d_n}{\Gamma} \quad (6)$$

From expression (2) the normalized lateral force is given by $\overline{F}_i$=1033x1 = 1033 kN and from expression (3) the mass of an equivalent SDOF system was determined as m^*=1033 ton . The results from expressions (4), (5) and (6) where Γ=1 , F^*=F_b and d^*=d_n The next step defines the yield displacement of the idealized SDOF system d^*_y through expression (7).

$$d_y^* = 2\left(d_m^* - \frac{E_m^*}{F_y^*} \right) \quad (7)$$

Through the previous expression: d_y^*= 0,212 m.

The image below (Figure 39) shows how to determine the values of F^*_y and d^*_m that correspond to the coordinates of point A on the capacity curve of the structure. Point A correspond to the formation of the plastic mechanism and E_y^* is the deformation energy up to the formation of the plastic mechanism (point A). The blue bilinear of Figure 40 corresponds to the third iteration that Figure 39 illustrates.

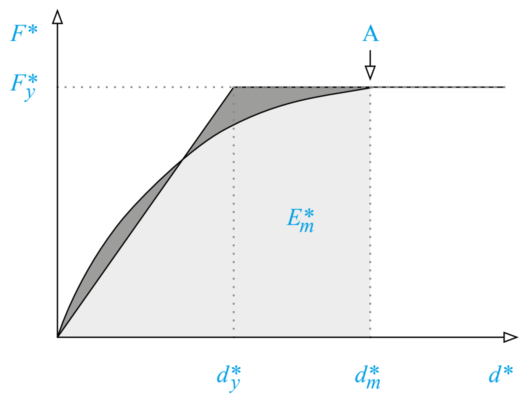

Figure 39 · **Determination of the idealized ratio/elasto-perfectly plastic displacement [52]**

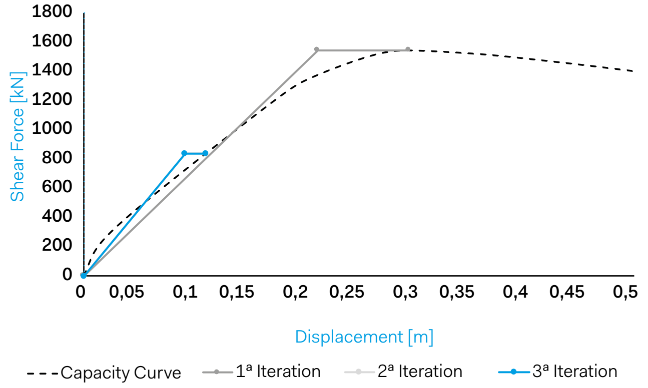

Figure 40 · **Capacity curve and iterations representation to determine the target displacement**

The next step was to calculate the period T^* of the idealized equivalent SDOF system, determined by expression (8) with the previous determined values m^*, d_y^* and F_y^*.

$$T^* = 2\pi\sqrt{\frac{m^* d_y^*}{F_y^*}}$$

(8)

The period corresponding to the 1st iteration, and by applying the previous expression, was:

$T^* = 0{,}212\ m.$

Finally, the determination of the target displacement of the equivalent SDOF system can be done through the determination of the elastic acceleration response spectrum at the period T^*, previously defined. The expression used to determine the target displacement was the (9) presented below. Once the structure was a longer period range ($T^* \geq T_C$) the target displacement $d_T^* = d_{et}$.

$$d_{et}^* = S_e(T^*)\left[\frac{T^*}{2\pi}\right]^2$$

(9)

By applying the previous expression:

$d^*_{et} = 0{,}111\ m.$

The value $S_e(T^*)$ is affected, in this case, by a coefficient of 0.75 according to Table NA.I presented on the Portuguese Annex of the Eurocode 8 – Part 3 [30]. This coefficient is to obtain the maximum reference acceleration related to Type 1 seismic action along with the severe damage (SD) limit state. According to the table previously referred, in cases where the Type 2 seismic action is more severe, a coefficient of 0.84 must be adopted.

An optional iterative procedure was still done in order to obtain an accurate target displacement. According to Annex B of Eurocode 8 – Part 1 [30], this iterative procedure is done when d_t is much different from the displacement d_m^*.The iterative procedure applied consisted on repeat the steps from expression (7) to (9), but considering the previously calculated d_t as d_m^*. F_y^* will be the corresponding value of d_t (d_m^*). In this case, three iterations were made, and the bilinear curves are presented in Figure 40: 1st iteration in the light grey line, 2nd in dark grey and the 3rd iteration and final in blue. The values resulting from the expressions (7) to (9) are those corresponding to the 1st iteration. The final value for target displacement was $d_t = 0.111\ m$. The iterative procedure was stopped once that $d_t = d_m^*$.This was the procedure applied to the other building direction.

6.6. Nonlinear dynamic analysis

The seismic assessment of the building's performance was also carried out through nonlinear dynamic analyses. According to Eurocode 8 – Part 1, a suite of at least 7 analyses should be carried out in order to define the seismic demand as the average of the analysis set. In the present study, 10 analyses were considered, corresponding to 5 different events, with each seismic component acting along with the two main horizontal directions of the buildings. Each analysis considers the ground acceleration acting simultaneously along with the two horizontal and vertical directions, corresponding to the accelerations recorded at the stations for each event.

The records were selected from the suit of nearly 3500 records included in a database of ground motions recorded in the Mediterranean region. The selection and scaling of each suit of accelerograms follow generically the strategy prescribed in Eurocode 8, i.e., the average spectrum of the selected ground motion should be higher than the code peak ground acceleration and higher than 90% of the code spectra along with the period interval between 0.2 and 2 times the fundamental period of vibration. Given that, the accelerograms are applied simultaneously along the two horizontal directions with accelerograms recorded also along with two directions, the average of the fundamental periods in the two directions (T_m) was adopted as reference period of vibration of the building (see Table 5), whilst the event spectra were defined as the geometric mean of the two horizontal directions of the recorded motion.

Additional constraints were also imposed to limit the scaling to a factor of 2.5 and to minimize the error in terms of maximum spectral accelerations. Figure 41 shows the comparison between the code acceleration spectrum for the Seismic Zone 1.3 in Portugal and the acceleration spectra associated with the selected records. The graphs include also the average of the selected spectra (thick dashed line), the reference limits corresponding to 90% and 130% of the code spectrum (thin dashed line), and the period interval of interest (shaded area).

Table 5 · Periods of vibration determined for the buildings in study

Building ID	Fundamental period of vibration – T (s)		T_m (s)	$S_e(T_m)$	$S_{De}(T_m)$
	x	y			
B3_ModC	1.50	1.96	1.73	1.68	0.096

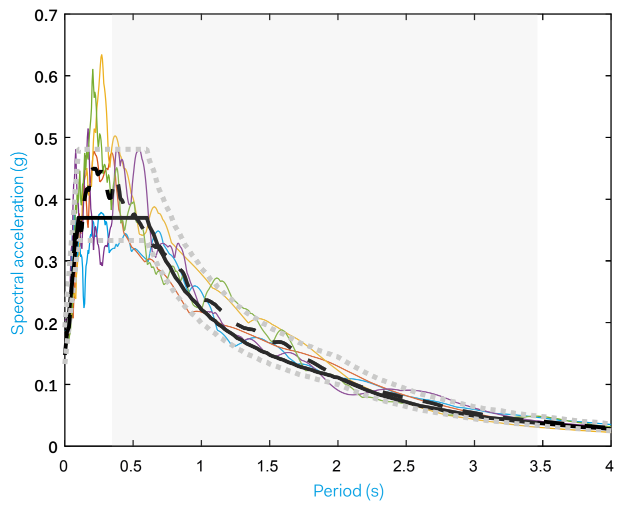

Figure 41 · Acceleration response spectra of the records selected to perform the nonlinear dynamic analyses for building B3_ModC

6.7. Buildings assessment

The results determined from both static and dynamic analysis are discussed in this section in view of the elements compliance with respect to Eurocode 8 – Part 3 capacity prescriptions, in terms of elements chord rotation and shear force.

6.7.1. Structural capacity

The capacity of the building elements was carried out in terms of chord rotation (deformation) and shear strength, whose values are shown in the Table 6, following the expressions proposed in Eurocode 8 – Part 3 [30]. The assessment was carried out for the significant damage (SD) limit state, for which, the chord-rotation capacity Θ_{um} is defined using the expression (10) presented below for convenience. In Table 6, the chord-rotation capacity values correspond to a front façade column, as an example.

$$\theta_{um} = \frac{3}{4}\frac{1}{\gamma_{el}} 0.016\left(0.3^{\vartheta}\right)\left[\frac{max(0.01;\,\omega')}{max(0.01;\,\omega)} f_c\right]^{0.225}\left(min\left(9;\,\frac{L_V}{h}\right)\right)^{0.35} 25^{\left(\alpha\rho_{sx}\frac{f_{yw}}{f_c}\right)}\left(1.25^{100\rho d}\right) \quad (10)$$

The symbols of the expression above are described in the Eurocode 8 –Part 3 [30]. In terms of shear strength of the RC elements, the capacity is given by expression (11).

$$V_R = \frac{1}{\gamma_{el}}\left[\frac{h-x}{2L_V} min(N;\,0.55A_c f_c) + \left(1-0.05\, min(5;\,\mu_\Delta^{pl})\right)\left[0.16\, max(0.5;\,100\rho_{tot})\left(1-0.16\, min\left(5;\,\frac{L_V}{h}\right)\right)\sqrt{f_c}A_c + V_w\right]\right] \quad (11)$$

The geometry and material properties to include in the previous expressions were defined based on the data collected from the original project and assuming a limited knowledge level (KL1) that, according to the code prescriptions, should reduce the material properties by a factor of 1.35. In the case of the building in study, the level of knowledge corresponds to the access of the original outline construction drawings with sample visual survey (geometry), the simulated design in accordance with relevant practice and from limited in-situ inspection (details) and regarding the materials, default values in accordance with standards of the time of construction and from limited in-situ testing. In some cases, full access to information on the mechanical properties of the building material was given.

The previous equations were applied only to the column given that for this typology of buildings, the beams should remain essentially undamaged. However, despite the code does not provide any specific consideration for PRC buildings, particular attention is given to the behavior of the beam-to-column connection, as it is one of the main focuses of damage in recent earthquakes. In this regard, a relative displacement limit of 8 cm was considered, a limit from which the connection suffers severe damage and requires intervention, suggested by Cornali *et al.*[8]

Table 6 · Capacity values calculated according to Eurocode 8 – Part 3 [30]

Building ID	Chord rotation [rad]		Shear strength [kN]	
	x	y	x [m]	y [m]
B3_ModC	0.038	0.039	5316	5733

6.7.2. Non-structural capacity

As is known and has been subjecting of debate, cladding panels are not considered structural elements. However, the damages that this type of elements suffered in a seismic scenario are also known and reported by several authors [2][5][16][53]. Cornali *et al*. [8] presented a work where a seismic assessment in an existing industrial building was done. The authors evaluated the safety and potential losses associated with seismic events, pointed the cladding panels as the most vulnerable element on the building in the study, and highlighted the significant impact on the estimation of the total repair cost. Another aspect of enormous importance in these elements is their high weight and that, in a seismic scenario, it represents a danger to the people, once their overturning to the out of the plane is one of the most reported damages related to the cladding panels [5]. For the reasons described above, in the assessment of the buildings, the damages states presented by Cornali *et al*. [8] for the cladding panels were taken into account. They are 1 cm of relative displacement for the panel damage limitation and correspond to the yielding of the top connections of the panel, and 4 cm to the panel collapse prevention that corresponds to the rupture of the connections and fall of the cladding panels. These values were multiplied by the number of panels considered in the building, whose values can be seen in Table 7. The points corresponding to the damage states of the panels are plotted in the result graphs on top of the uniform pushover curves with an orange and red circle for damage limitation and collapse prevention, respectively.

Table 7 · Panels damage states values

Building ID	Number of horizontal panels	Panels damages states [relative displacement in cm]	
		Damage Limitation	Collapse Prevention
B3_ModC	3	3	12

6.7.3. Static analysis

The results of the pushover analysis are presented in Figure 42, showing the capacity curves in X and Y directions (solid and dashed lines, respectively) associated with the uniform and modal load distributions (red and green lines, respectively), as well as these distributions affected by the accidental eccentricity (dark and light grey lines for uniform and modal analysis, respectively).

The first conclusion regards the almost perfect overlapping of the pushover curves associated with the uniform and modal distributions, which is associated with the fact that the structure is single-story building and regular in plan.

Regarding the seismic safety assessment (Figure 42), the building appears to fulfill the code requirements, given that the target displacement (green square represented in pushover curves) associated with the seismic zone 1.3 is lower than the displacement associated with the exceedance of the elements chord rotation (red triangle represented in pushover curves for chord rotation capacity) and shear capacity (Table 6). The latter mechanism, contrary to what is commonly observed in conventional RC buildings, is very unlikely to occur given the large slenderness of the columns. Hence, based on the code requirements, the building could be classified as seismically safe.

Similar results were attained considering the behavior at the beam-to-column connection. The building does not seem to have problems with the beam-to-column connections level. However, at the level of the connections between the panels and the columns, there seem to be some problems identified by the large difference between the panel damage limitation (orange circle) and the target displacement (green square). It can also be verified that the point that corresponds to the panel collapse (red circle) is quite close to the target displacement despite being slightly higher, but it is located before the displacement associated with the ultimate chord rotation (red triangle), pointing for a collapse of the panels for moderate to higher seismic forces.

Seismic Precast ///

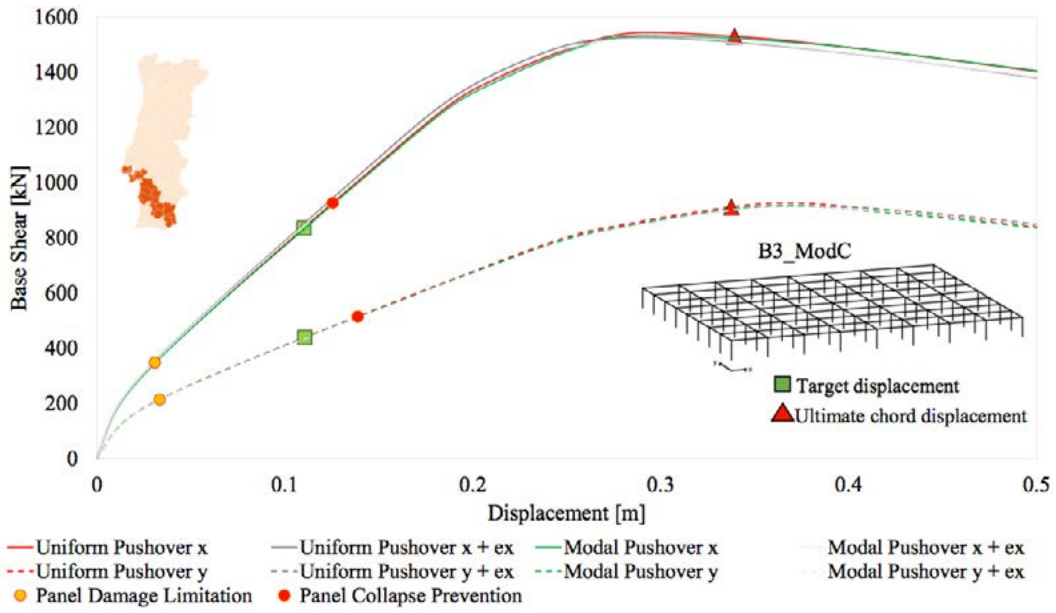

Figure 42 · Pushover curves for x and y direction for building B5_PreC

6.7.4. Dynamic time history analysis

This section discusses the results of the dynamic analyses comparing with the capacity curves obtained with the uniform load distribution, for both for X and Y directions (Figure 43). In this figure, the dark grey circles represent the response in the X direction and the light grey represents the response along Y direction. It is noted that these points represent the combination between the maximum base shear and the maximum top displacement that the structure experienced during the analyses, which may not necessarily be coincident in time nor be representative of a given structural state. Yet, for the sake of assessment and comparison with the pushover curves, these represent an admissible metric.

The pushover curves generally present a good agreement with the set of records used to perform the dynamic analysis. Yet, it is noted that most of the dynamic points present a larger displacement and base shear with respect to the target displacement obtained in the static procedure. Part of the differences are certainly justified by the conservative rules considered in the selection of records compatible with the

code spectra. Nonetheless, the response measured during the dynamic analysis is, in some cases, significantly higher, indicating that the use of nonlinear static procedures appears to underestimate the seismic demand. For instance, the mean value of the dynamic analyses' response (blue diamond in Figure 43) is well beyond the target displacement obtained with static analyses.

Regarding seismic safety, the results indicate that the building in the study is safe with respect to the prescriptions defined in Eurocode 8 – Part 3, in terms of columns shear and chord rotation capacity.

In terms of beam-to-column connections, the moderate code building in the study does not present any apparent problems in terms of the imposed actions. The same cannot be concluded regarding cladding panels. Regarding the damage limits of the panels, particularly with respect to damage limitation, the displacements of all dynamic analyses are exceeded, and only a few analyses do not reach the limit of collapse prevention, as presented in Figure 43. Thus, it is verified deficient behavior of the building regarding the limits of non-structural elements.

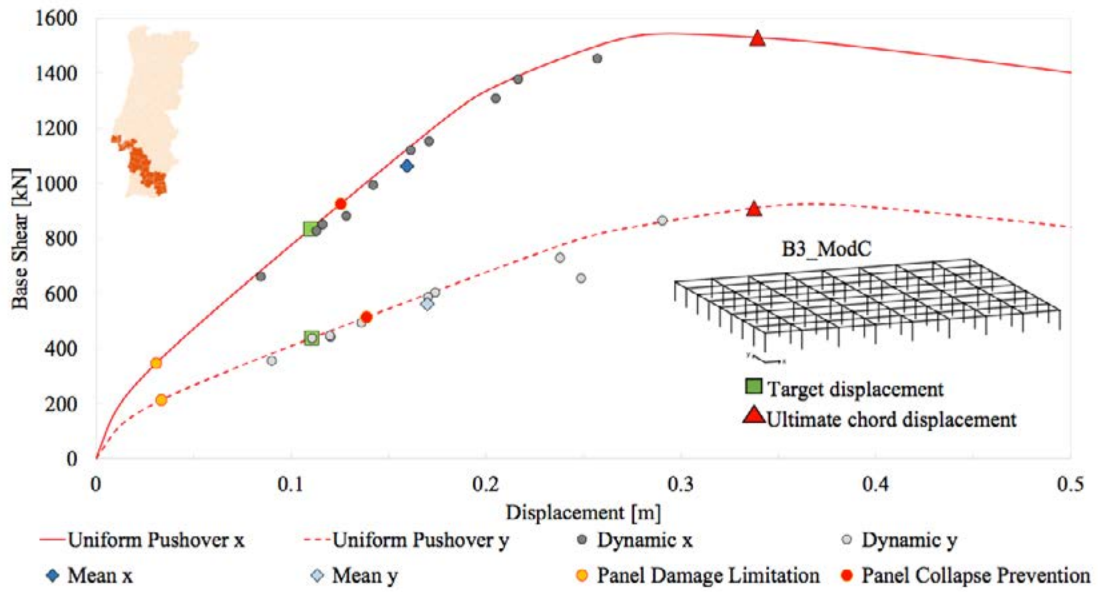

Figure 43 · Dynamic results for x and y direction for building B3_ModC

7. Risk assessment

7.1. Introduction

Seismic risk studies are of paramount importance to provide meaningful and useful information to property owners and public authorities in terms of the expected casualties and economic losses or disruption times [54]. Although the seismic risk in Portugal has been documented over the past few years in studies applied to residential buildings [55], [56], or schools [57], none addressed the impact in the industrial building stock. Besides, the damage observed in the PRC buildings after past earthquakes (e.g., Marmara (Turkey) in 1999, Lorca (Spain) in 2011, Emilia Romagna (Italy) in 2012), exposed important vulnerabilities in the structural and non-structural components, related with the insufficient columns' capacity and inadequacy of the beam-to-column connections, as well as due to weak connections between the cladding panels and the main structure.

Seismic risk analysis comprises the convolution of three main components: seismic hazard at the sites of interest, the exposure or the socio-economic value at risk, and the vulnerability of the values exposed to the seismic hazard. The integration of the different parameters and seismic risk calculations were carried out using the *OpenQuake-engine* [58], [59], an open-source seismic hazard and risk calculation software supported by the Global Earthquake Model Foundation.

7.2. Hazard

In the present study, two different earthquake scenarios, representative of the most relevant seismic sources in Portugal were considered as a baseline to assess the potential losses in the PRC building stock in the country: a strong magnitude offshore event associated with the Euroasian-African interplate and an onshore intraplate rupture at the Tagus Valley fault. The rupture parameters adopted for these scenarios are summarized in Table 8, and were defined based on the parameters proposed by Silva & Paul [60].

Table 8 · **Rupture parameters adopted for the different earthquake scenarios**

Rupture	Magnitude (MW)	Coordinates	Strike	Dip	Rake
Offshore	5.7	38.82N; 9.05W	220°	55°	0°
Offshore	8.7	36.9N; 9.9W	35°	40°	90°

For each of the abovementioned seismic scenarios, 1 000 ground motion fields were generated to properly propagate the aleatory uncertainty in the ground motion models into the loss results. The spatial distribution of the median PGA (in g) for mainland Portugal is depicted in Figure 44 for both earthquake ruptures.

Seismic Precast ///

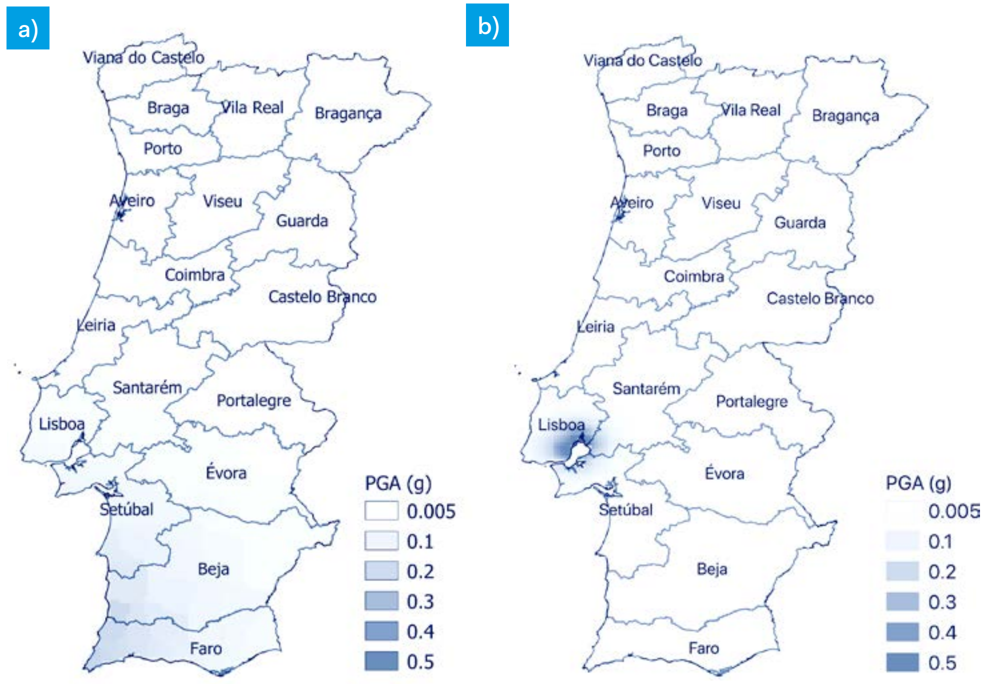

Figure 44 · **Mean ground motion fields for a) the offshore and b) onshore scenario**

7.3. Exposure

The exposure model comprises the spatial distribution of PRC buildings in the Portuguese mainland territory. The distribution of the building stock follows the data collected by Crowley *et al*. [61], which is in good agreement with the buildings percentage and geographic distribution presented in previous studies carried out by Sousa *et al.* [62] and Rodrigues *et al*. [47]. According to Crowley *et al.* [61], only nearly 12% of the industrial area corresponds to PRC buildings, representing about 6 938 buildings with an average area per building of approximately 1 032 m^2. In terms of spatial distribution, it is possible to observe a concentration of industrial facilities in the north of the country and along the coast, as illustrated in Figure 45.

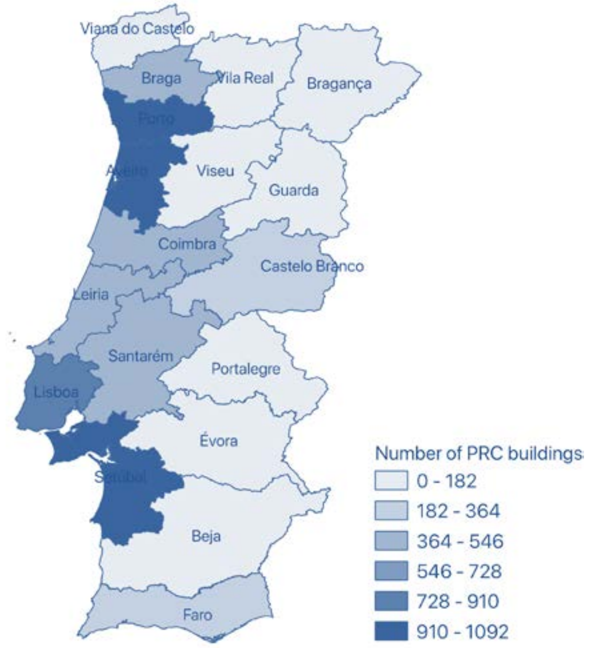

Figure 45 · **Distribution of PRC buildings in Portugal according with Crowley *et al.* [61]**

In terms of potential losses, it is assumed that 50% of the contents and inventory can be recovered even if the building suffers complete damage. The disaggregation of the value of the assets adopted in this study is depicted in Figure 46. Furthermore, the losses expected whenever the moderate damage limit state is achieved were set to one-tenth of the ones attributed to the complete damage, as recommended in HAZUS [63].

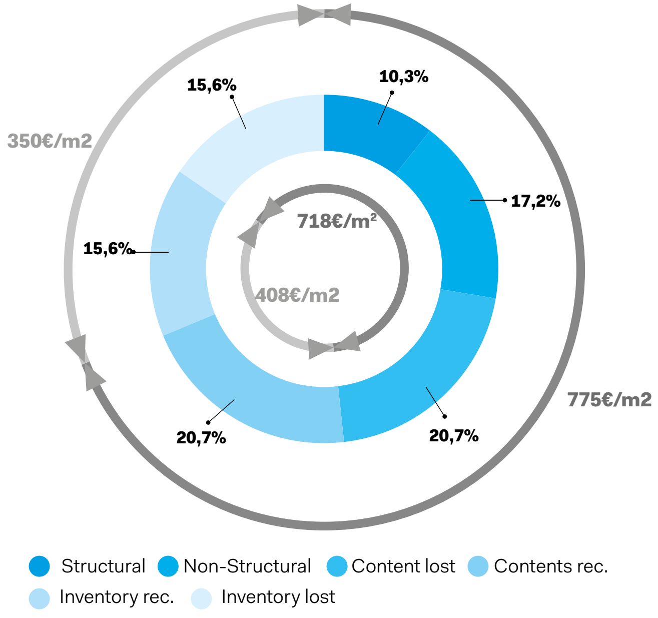

Figure 46 · **Disaggregation of the assets value**

Regarding the population exposed, according to the Statistics of the Industrial Production 2019 [64], each industry company had an average of 10.9 people in 2019. Under the assumption that on average each building corresponds to one company, this leads to approximately 75 624 people working on PRC buildings. Based on these hypotheses, we considered an average of 0.01 employees per square meter, considering an average area per industrial facility of 1032 m^2.

7.4. Structural fragility

The fragility functions in terms of structural and non-structural components were defined based on the numerical study carried out by Sousa *et al*. [65] based on a population of hundreds of synthetic buildings generated based on the geometric properties gathered from dozens of existing industrial PRC buildings in Portugal (see Chapter 3). In order to reflect this observation, which seems to be naturally related to the evolution of the construction processes, the properties were sampled according to the flowchart presented in Figure 47.

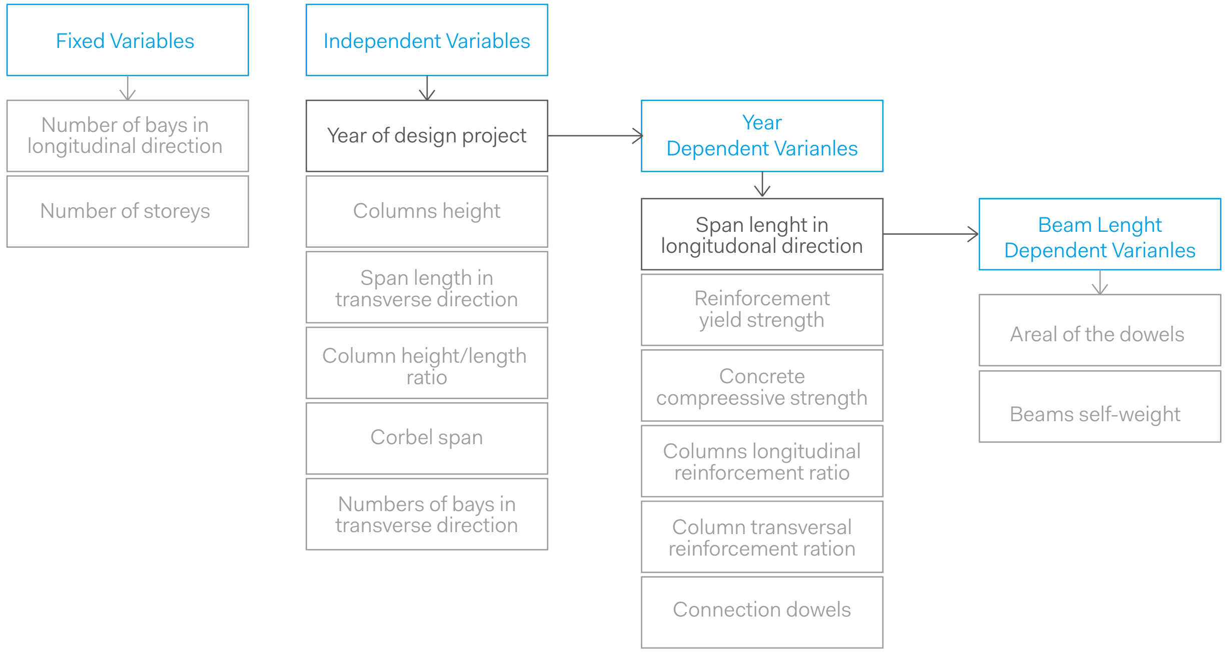

Figure 47 · **Properties considered in the model generation**

Considering the larger variability in the building geometric properties when compared to the ones observed in conventional residential buildings (e.g. [66], [67]), a total of 1000 industrial buildings were considered in the numerical study. Despite the observed relation between the dowel area and the span in the longitudinal direction, the buildings built before 1990 were modeled without steel dowels. The data collected does not permit the identification of a clear threshold for the generalized use of steel dowels. However, this year seems appropriate as it corresponds to the introduction of a modern seismic code in Portugal (i.e., 1983 – RSA [68]), with an additional period of dissemination and implementation in practice. In the buildings with steel dowels, the connections of the columns to both longitudinal and transverse beams consider two dowels, as these are the typical values found in this type of industrial buildings. Given the lack of specific codes addressing the design of PRC buildings in Portugal, it was decided to define three sub-classes based on the year of construction, as an important fraction of the mechanical and geometric properties depend on the year of construction. The three groups were defined as Pre-Code (1960-1980), Moderate-Code (1980-2000), and Post-Code (2000-2020), as depicted in Figure 48.

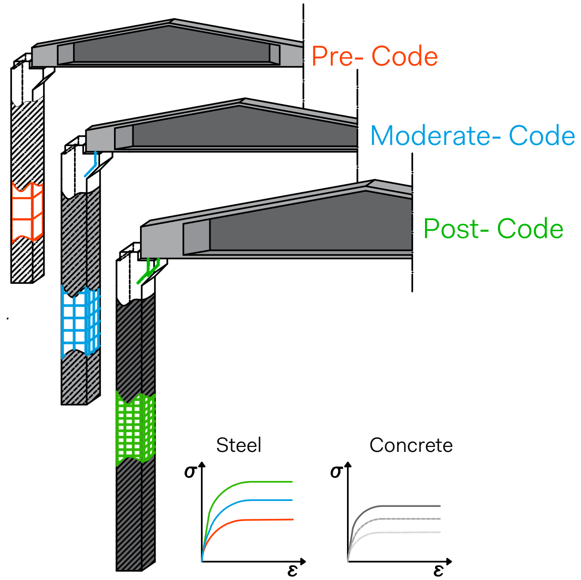

Figure 48 · **Schematic illustration of the building properties associated with the different periods of construction**

In order to understand the contribution of the different mechanisms to the seismic behavior of these structures, every building was simulated with three variants of beam-to-column connections: (1) pinned connection, (2) connection with dowels, and (3) connection without dowels. The latter two cases were simulated with the macro-model described in Section 4.2. As expected, this variation leads to distinct seismic behaviors of the overall structure. As illustrated in Figure 49, in the absence of steel dowels, the seismic coefficient (defined as the ratio between the lateral strength and the self-weight of the building) is largely reduced to a maximum value of about 0.1.

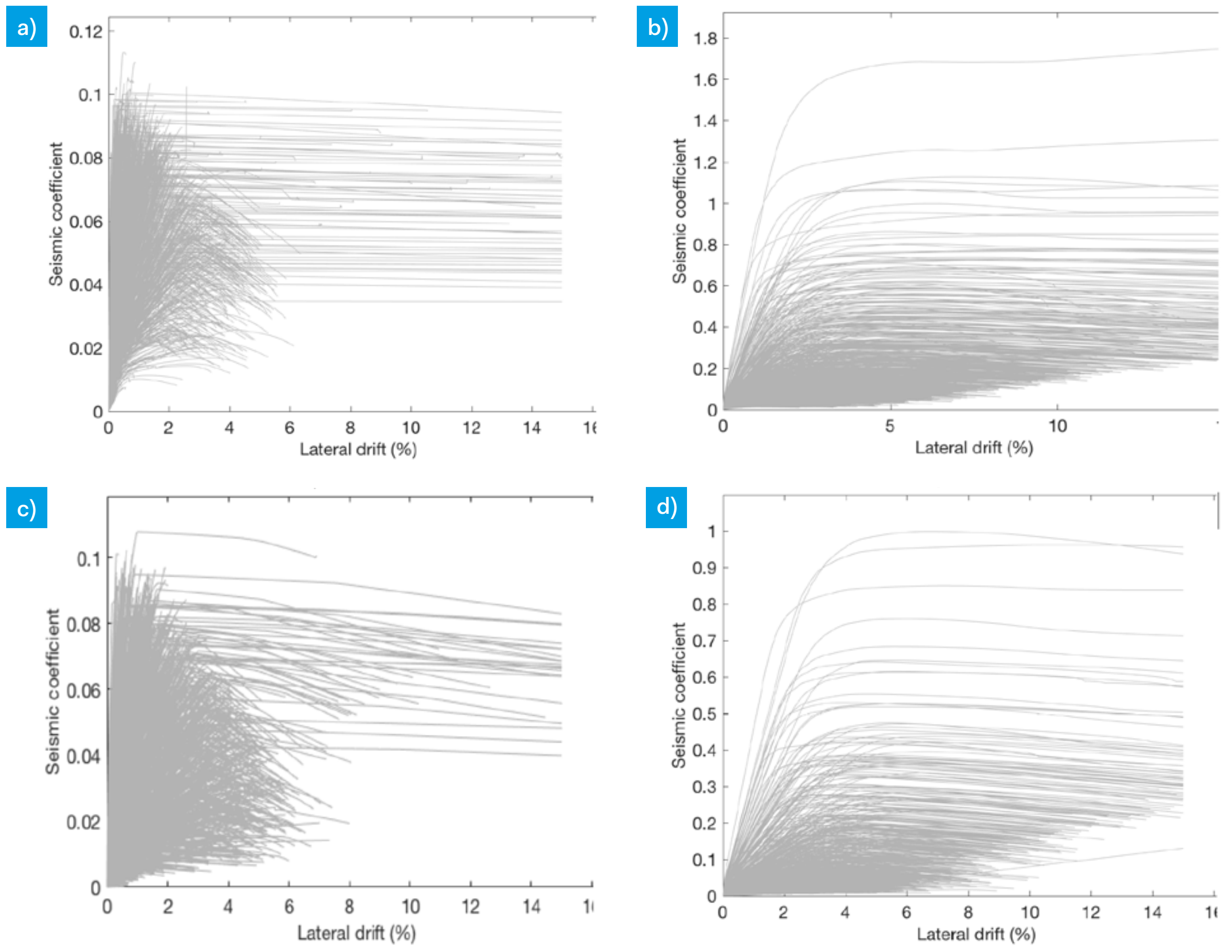

Figure 49 · Relations between lateral drift and seismic coefficient along a) X- direction without dowels, b) X- direction with dowels c) Y- direction without dowels and d) Y- direction with dowels

Following the results obtained, three different classes of buildings were considered, reducing the variability of the structural properties within each group. Each of these groups includes 300 buildings (analyzed in both directions), which was found to be enough to obtain convergence in the structural response. Only buildings built after 1990 were

assumed to have steel dowels at the beam-to-columns connections. This implies that the three groups will reflect different dowel properties: (1) no dowels for pre-code buildings, (2) half of the buildings with dowels for moderate-code buildings, and (3) all buildings with dowels for post-code buildings.

The seismic performance of every building was assessed considering a dataset with 250 records covering the Mediterranean region, which is consistent with the region under study. Considering the large period of vibration characteristic of this type of structure, all the records were scaled considering a maximum factor of 3.5 in order to reach seismic intensities capable of causing the structures to collapse. The scaled acceleration spectra together with the histograms of the peak ground acceleration and spectral acceleration at the average period of the synthetic building portfolio (T = 1.7 s) are presented in Figure 50. It is noted that the magnitude and dispersion of the fundamental periods are essentially independent of the period of construction. The seismic performance of each building was then accessed through the N2 method [69], as suggested in Eurocode 8, along the two directions of the buildings.

A key step in the derivation of fragility functions involves the definition of the thresholds for the EDPs, representing different damage levels. For the fragility analyses presented herein, two limit states were considered: damage control and collapse prevention, associated with both structural and non-structural components. A summary of the adopted structural and non- structural limits states is presented in Table 9.

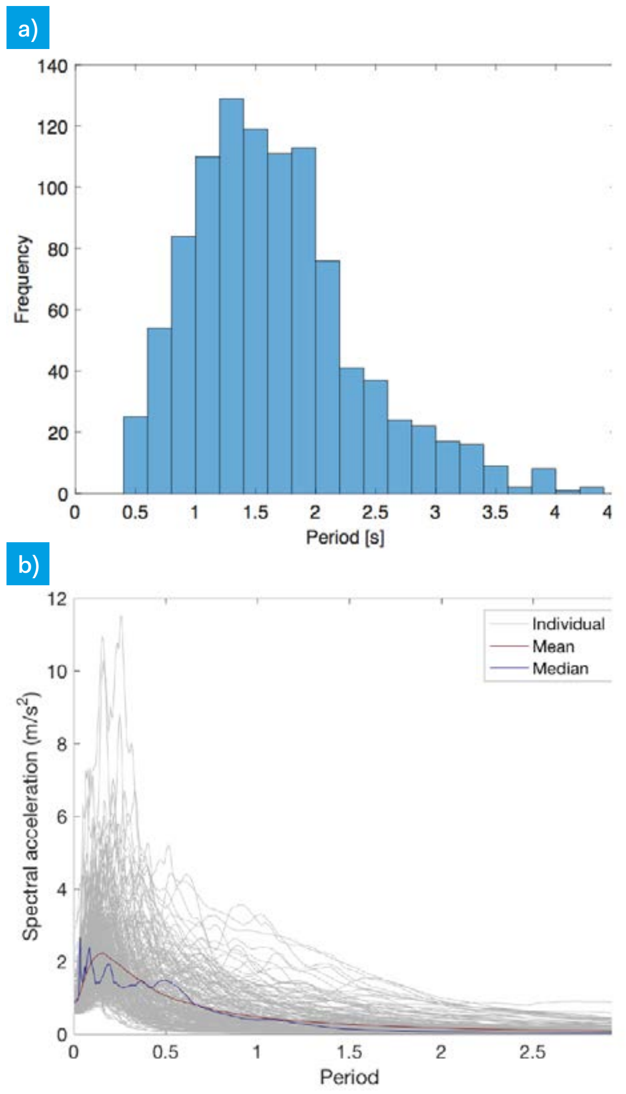

Figure 50 · Effect of buildings dynamic properties in the seismic hazard: a) histogram of the average period of both building directions and b) scaled spectral accelerations considered as seismic input

Table 9 · **Limit states adopted for the different elements and performance levels**

Structural limit states		
Columns	Collapse prevention	80% drop Fmax
	Damage limitation	60% Fmax
Connection	Collapse prevention	8 cm relative displacement [8]
	Damage limitation	3 cm relative displacement [8]
Non-structural limit states		
Claddings	Collapse prevention	4 cm relative displacement between cladding connections [8]
	Damage limitation	1 cm relative displacement between cladding connections [8]

The fragility functions were derived using a nonlinear static procedure carried out on 900 synthetically generated numerical models, equally distributed across the 3 different building classes. Considering that each building was analyzed along with the two directions, the seismic intensity associated with each building (averaged spectral acceleration at the average elastic period of all the buildings (T=1.7 s)) was defined based on the minimum of the one obtained for each direction.

The results presented in Figure 51 show the response of the individual industrial buildings together with the associated lognormal cumulative distribution associated with the structural limit states (i.e., damage limitation and collapse prevention) for the three building classes, disaggregated in terms of conditioning mechanism (columns or connections). Each point in the plots represents the ratio of buildings within each class that reached a given limit state under analysis for each ground motion record, represented by the associated averaged spectral acceleration.

The results confirmed that, in the presence of dowels, the response is generally controlled by the columns, while the failure at the connections is observed only in marginal cases (bottom plots in Figure 51). On the contrary, in the absence of steel dowels (in all the Pre-code buildings and a fraction of the Moderate-code buildings), a larger number of buildings exhibit vulnerabilities at the connection level. The reason for this distinct behavior relies on the reduced lateral strength of the columns analyzed in this study. In the presence of particularly slender columns, the response tends to be governed by the columns' behavior and the friction strength at the connection level is often enough to sustain the maximum shear forces developed in the columns. For the cases where the columns are more robust (with a local seismic coefficient higher than about 0.1), the friction at the connection is not enough to sustain the lateral loads and the beams experience large lateral displacements.

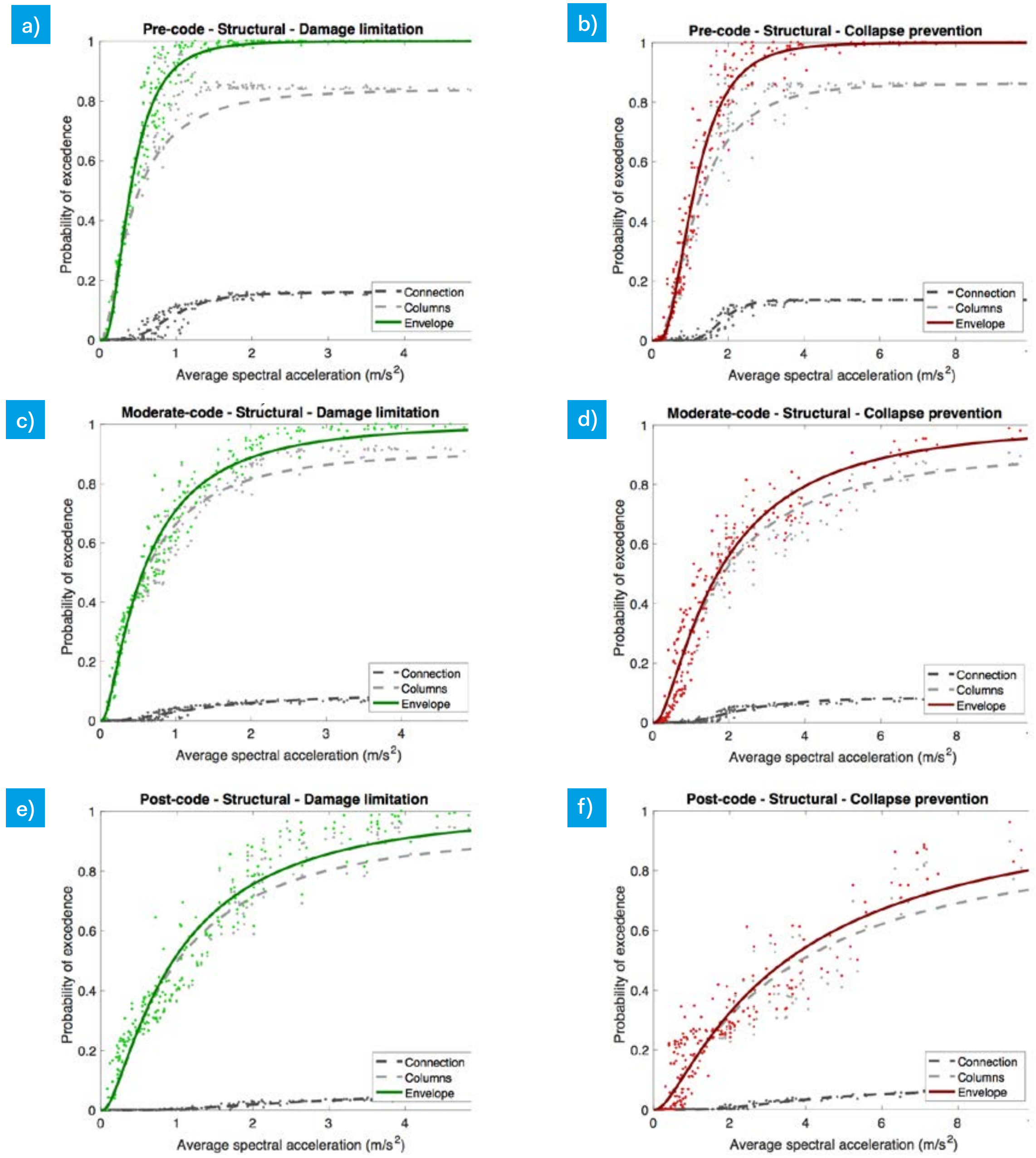

Figure 51 · Structural fragility functions for building models for a) Pre-code design for damage limitation state, b) Pre-code design for collapse prevention limit state, c) Moderate-code design for damage limitation state, d) Moderate-code design for collapse prevention limit state, e) Post-Code design for damage limitation state, f) Post-Code design for collapse prevention limit state

Seismic Precast ///

For what regards the non-structural components, all the typologies presented similar average spectral accelerations for both limit states and, therefore the results presented reflect the behavior of the entire portfolio of buildings (see Figure 52). The reduced variation observed among the different groups results from the columns' slenderness (and hence the building's initial lateral stiffness) being independent of the year of construction. Furthermore, given the low deformation level associated with these limit states, the damage in the cladding appears to be independent of the type of structural failure.

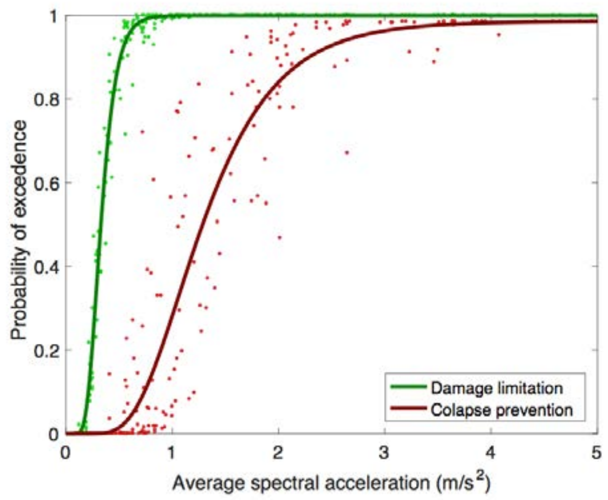

Figure 52 · **Non-structural fragility functions for building models from all ages**

The most relevant statistical parameters of the fragility curves are presented in Table 10, for average spectral accelerations. The statistical parameters of the lognormal distributions present an acceptable correlation with the individual data with correlation values R^2 higher than 0.9 for all the curves presented in this work.

Table 10 · **Summary of the statistics associated with the fragility functions in terms of averaged spectral accelerations in m/s²**

Limit state		Pre-code		Moderate-code		Post-code	
		Mean	Stdv	Mean	Stdv	Mean	Stdv
Structural	Damage limitation	0.50	0.37	0.97	1.37	1.69	2.48
	Collapse prevention	1.33	0.87	2.92	4.07	7.35	13.78
Non-structural	Damage limitation	0.35	0.14	0.35	0.14	0.35	0.14
	Collapse prevention	1.50	0.77	1.44	0.68	1.40	0.63

7.5. Loss Assessment

Damage in industrial buildings is responsible for large social and economic consequences. As noted by Liberatore *et al*. [4] and Magliulo *et al*. [5], after the 2012 M6.2 (20 May) and the 5.8 (29 May) Emilia-Romagna earthquakes, hundreds of industrial facilities suffered severe damage and up to 7000 people lost their jobs due to the direct and indirect effects of the main earthquake and subsequent aftershocks. The economic losses were estimated as 1 billion EUR on direct losses and about 5 billion EUR on indirect losses due to the disruption of production. In Turkey, after the 1999 M7.6 Kocaeli earthquake, economic losses related with the industrial activities were estimated in more than 30% of the Turkish Gross National Product, corresponding to between 9 and 13 billion USD, decomposed in 5 billion for buildings, 2 billion for industrial facilities, 1.4 billion for infrastructures and the remaining losses for economic losses related with the normalization of the industrial facilities to their normal production levels [70].

7.6. Economic indicators and cross-sector exchange model

The quantification of the indirect losses considered two main indicators: the geographic location of each economic activity and the interconnections between the economic sectors that develop their activity in PRC buildings or are likely dependent on sectors whose activity is developed in this type of buildings. The values described in Table 11 present the distribution of the different economic activities at the NUTS II regions reported in 2019.

Table 11 · Location of the most relevant economic activities, in %, according to the Portuguese Statistical Office based on data collected in 2019

	Agriculture	Industry	Construction	Trade & Transport.	Total
North	10.2	7.0	6.0	17.3	40.6
Centre	5.9	3.3	4.6	10.7	24.5
MAL	1.6	2.0	4.0	12.7	20.3
Alentejo	3.9	0.8	0.9	3.2	8.8
Algarve	1.2	0.0	1.3	2.4	4.8

Given the interdependencies between the various sectors, eventual direct losses affecting a given sector might generate constraints in both shipment and purchases to other economic sectors. This effect can be represented in input-output matrixes, such as the one presented in Table 12, showing the exchanges measured in Portugal in 2013. These values refer to the total industrial building stock. For the purpose of this study, those were multiplied by 12% to represent the expected portion of economic activity in PRC buildings. Each column quantifies the contribution that a given sector has for the sector identified in the first row plus other payments (including taxes) and importations. On the other hand, each row indicates the production of that sector to the different sectors identified in the columns, plus the demands from consumers and exports.

Table 12 · Cross-sector exchange of products in Portugal in 2013 in million EUR (adapted from INE [71])

Sector	Agriculture	Industry	Construct.	Trade & transport	Other demands	Export.	Total
Agriculture	1 023	6 284	1	444	5,313	1,029	14 094
Industry	2 441	44 177	4 854	12 695	60 258	45 851	170 276
Construction	104	335	5 037	1 411	12 153	651	19 691
Trade & transport	566	7 029	1 801	39 756	67 549	10 956	127 657
Other payments	6 675	109 166	4 713	70 066			190 620
Import.	3 285	3 285	3 285	3 285			13 140
Total	14 094	170 276	19 691	127 657	145 273	58 487	522 338

7.7. Direct losses

The outcome of the seismic risk analysis revealed distinct results for the two scenarios. Even though the offshore seismic source is located at a larger distance from the regions of higher industrial activity, it potentially generates higher losses. This is due to the higher magnitude of the event and the fact that it produces larger spectral acceleration for longer periods of vibration (where the dynamic properties of the PRC buildings typically lay - Rodrigues *et al.*, [72]). For this reason, it is not surprising that the direct losses expected for the offshore scenario are nearly 10 times higher, totalizing approximately 0.35% and 0.04% of the Portuguese annual gross domestic product (GDP). The difference in the losses observed is partly related to the large geographical distribution of the losses throughout the country (see Figure 53). As previously noted, there is a large concentration of industrial facilities in the northern region of Portugal where, notwithstanding the distance to the epicenter, is subjected to non-negligible spectral accelerations due to the reduced attenuation observed for longer periods.

Seismic Precast ///

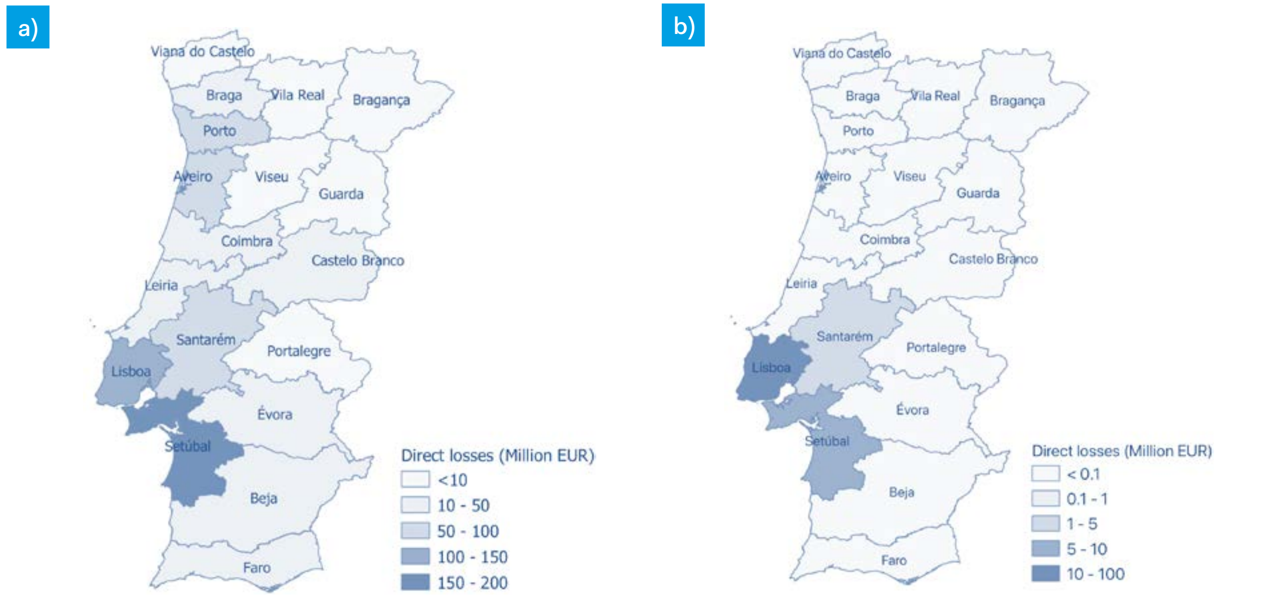

Figure 53 · **Distribution of the direct losses for the offshore (a) and onshore (b) scenarios**

The disaggregation of the losses by the period of construction and loss component shows a distinct behavior for the two scenarios considered. Regardless of the scenario considered, the results presented in Figure 54 show a consistent reduction in the structural, contents and inventory losses with the evolution in the design and construction processes. The significant reduction in the structural losses from the pre-code to the post-code is associated with the presence of steel dowels at the beam-to-column connections, as well as with the increase in the longitudinal and transverse reinforcement ratios (Rodrigues *et al.*, [25]).

On the other hand, it is observed that the losses related to the non-structural components remain essentially unchanged with the type of code in practice. This is already anticipated, as the fragility functions consider that the non-structural damage measured is essentially independent of the period of construction. It is worth noting that, notwithstanding the overall losses being higher in the offshore case, the losses associated with contents reach a higher value in the onshore case. In locations close to the rupture, the spectral accelerations tend to be amplified in the short period range, which had a strong correlation with damage in contents. On the other hand, for the offshore case, a higher amplification is expected for longer periods while PGA tends to attenuate faster with the increase in distance from the rupture.

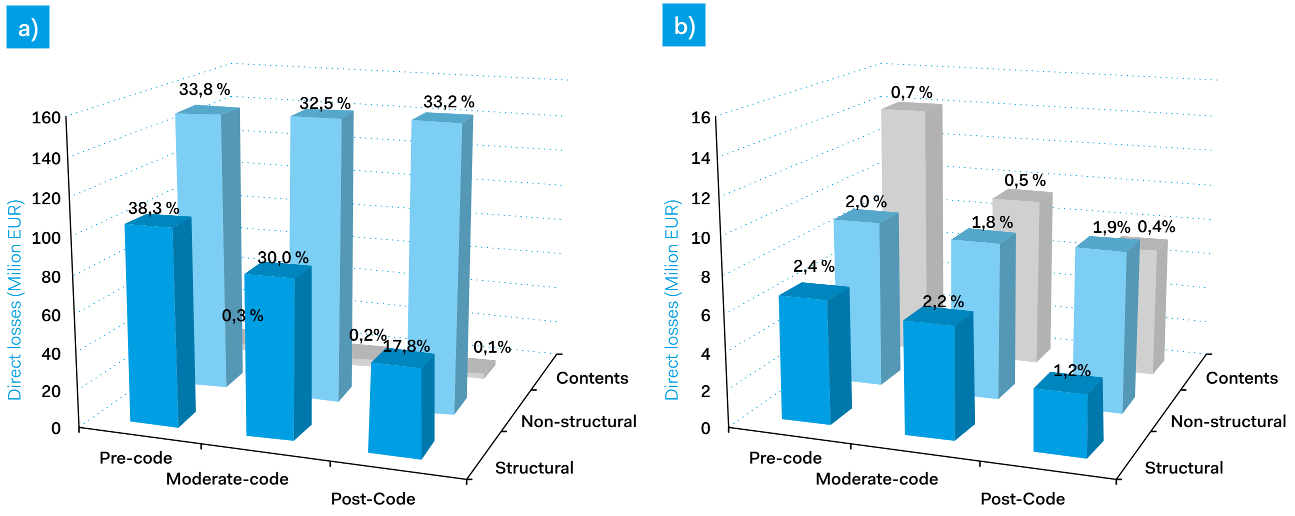

Figure 54 · **Distribution of direct losses for the offshore (a) and onshore (b) scenario disaggregated by period of construction and building components.**

In terms of human losses, for an industrial environment, a larger number of employees is expected during the day (80% of the exposed population), while during the night and transition periods, lower values are expected (10% and 50%, respectively). Following these occupation ratios, Table 13 presents the expected casualties for the two scenarios.

Table 13 · **Expected human casualties for the different scenarios and of time of the ground shaking**

	Day		Transition		Night	
	Injuries	Fatalities	Injuries	Fatalities	Injuries	Fatalities
Offshore	577	214	361	134	72	27
Onshore	34	13	21	8	4	2

7.8. Indirect Losses

The indirect losses encompass the costs associated with the business interruption, as well as losses due to the disruption of the economy. Other factors associated with the disruption in the education process, healthcare services, tourism, among others, were not included in this study due to the difficulties in quantifying these contributions with reliable metrics.

Based on the expected direct losses presented in the previous section and the information provided in Table 11, we computed the losses associated with the different economic sectors (see Table 14). In addition to the losses determined for each region, this table includes also the loss ratio at the national level (last column), reflecting the combination of losses and exposure at the different regions.

The losses estimated for each economic sector can then be used to update the initial exchange matrix presented in Table 12 estimates the economic losses caused by the constraints in the exchanges between the different sectors. It should be noted that this new tentative matrix (Table 15) represents only the contribution of the companies whose activity is developed in PRC buildings, i.e., 12% of the total industrial building stock. Moreover, was noticed that the model assumes that importations and exports can temporarily increase to compensate 50% of the unbalanced purchases and shipments, on the basis that Portugal can be considered an open market economy. This implies that part of the excess of production is not absorbed by the different internal economic sectors nor exported and will be temporarily accumulated in the companies' stocks.

This analysis revealed also that the impact of the indirect losses reaches regions that go much beyond the areas directly affected by the earthquake. This is because the different economic sectors are unequally distributed along the different regions, together with the growing trend for the opening of the economy and the interdependence between sectors, often located in different regions of the country or even in other countries. The data presented in Table 16 shows a spread in losses to regions not directly affected by the ground shaking, namely to the "Norte" and "Centro". This is one of the reasons that contribute to the indirect losses to eventually surpass the direct losses, as illustrated in Figure 55 for both seismic scenarios.

Table 14 · **Distribution of the expected direct losses in industrial facilities for the different regions and economic sectors, considering the onshore event, in ‰.**

Region	Direct losses at the regional level	Economic sector				Direct losses at the national scale
		Agriculture	Industry	Construct.	Trade & transport	
Norte	0.0	0.0	0.0	0.0	0.0	0.0
Centro	1.0	0.1	0.0	0.1	0.1	0.2
MAL	43.0	0.7	0.9	1.7	5.5	8.7
Alentejo	3.0	0.1	0.0	0.0	0.1	0.3
Algarve	0.0	0.0	0.0	0.0	0.0	0.0
Sum		0.9	0.9	1.8	5.7	9.2

Table 15 · **Cross-sector exchange of products in Portugal after the direct losses caused by the onshore scenario, in million EUR**

Sector	Agriculture	Industry	Construction	Trade & transport	Other demands	Export.	Total
Agriculture	123	753	0	53	637	123	1,690
Industry	293	5 296	581	1 515	7 224	5 499	20,408
Construction	12	40	603	168	1 456	78	2,358
Trade & transport	68	839	215	4 744	8 060	1 307	15,232
Other payments	800	13 088	565	8 360			22,813
Import.	394	394	394	392			1,573
Total	1 689	20 410	2 358	15 232	17 377	7 007	64,074

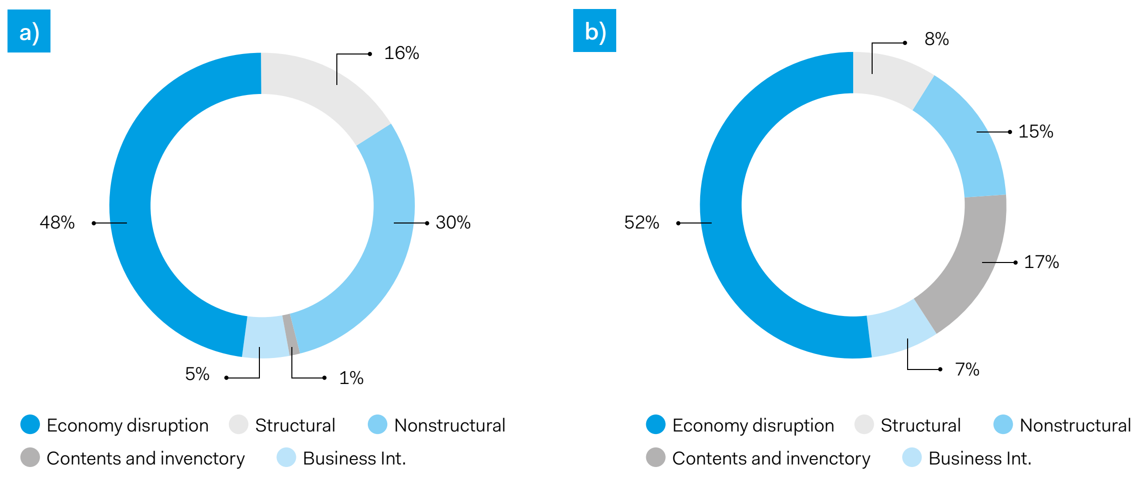

Figure 55 · **Distribution of the direct and indirect losses for the offshore (a) and onshore (b) scenarios**

Table 16 · **Distribution of indirect losses in the regions affected by the earthquake (local) and throughout the different regions of the country (global) in the subsequent period, during recovery, in ‰**

Region	Local indirect losses	Global indirect losses
Norte	0.0	0.4
Centro	0.2	0.5
MAL	8.7	8.9
Alentejo	0.3	0.3
Algarve	0.0	0.0

Despite the effort made to build up a reliable model to quantify indirect losses, the uncertainties associated with the type of economy (closed or open), labor mobility, supply chains or the potential for product substitutions due to relative price changes, call for special attention in the interpretation of the results. In addition, the results do not account for the financial condition of the firms and the dependency of firms on households that, according to Nasserasadi *et al.* [73], are particularly important for the assessment of indirect losses. For these reasons, the global figures presented in Table 17 are possibly a lower-bound estimation of the potential losses. Nonetheless, it is recalled that they refer only to the population of PRC buildings, and not entire industrial building stock.

Table 17 · **Summary of the losses estimated for the two scenarios**

	Direct		Indirect		Total	
	million EUR	% GDP	million EUR	% GDP	million EUR	% GDP
Offshore	700	0.35	790	0.39	1 500	0.74
Onshore	72	0.04	104	0.05	176	0.09

8. Final comments

The present document summarizes the work carried out under the SEISMICPRECAST research project.

After a detailed analysis of the main causes of damage observed in past events, this document presented the results of a survey carried out to compile the properties of 73 design projects of existing PRC buildings. Based on the information collected, it was possible to characterize, from a statistical point of view, the most relevant structural properties of the buildings in Portugal.

In addition to the geometric and mechanical properties of the buildings, an experimental investigation on beam-to-column connections was undertaken featuring the main configurations found in the PRC industrial buildings. The test was performed considering cyclic loads at the connection in order to simulate pure shear loadings. This work allowed us to observe the poor performance of the connections without any mechanical connector (dowel) and that the specimen with the dowels closer to the corbel face presented earlier damages compared to specimens with more centered dowels. Furthermore, it was observed more damage in the specimens without any neoprene between the concrete faces, although the strength remains essentially unchanged, pointing to the importance of these elements in the connections.

The data collected in the experimental tests together with additional information from previous tests allow the development and calibration of a simplified macro-model capable of accurately describing the main mechanisms involved in beam-to-column connections subjected to seismic loads. The proposed numerical approach accounts for the different load transfer mechanisms, namely the dowel effect, friction between the contact surfaces, and the deformability of the neoprene pad, and can be used to simulate the beam-to-column connections in nonlinear numerical analysis software packages.

This novel element was used in a parametric study to evaluate the importance of each component and its relative contribution to the seismic behavior of the entire structure. The results of both nonlinear static and dynamic analysis on existing buildings show that in the presence of adequately designed dowels, small deformations are expected at the connections level, and therefore the response of such structures is controlled by the properties of the columns. For these cases, the consideration of a simple pinned connection appears to be an efficient and accurate numerical approach. On the other hand, in the absence of dowels, or in cases where these are not properly designed, a concentration of damage is expected to occur at the connection level, whilst the columns remain essentially undeformed, which is in line with the damage observed in field observations after recent earthquakes.

This model was used to assess the seismic performance of existing buildings from different periods of construction from 1978 till 2018, and with different assessment procedures. It was verified that, regardless of the type of analysis considered, in regions of moderate seismicity the buildings appear to exhibit a satisfactory behavior when analyzed through the expressions proposed by Eurocode 8 – Part 3 to assess the column's performance. However, in the absence of steel dowels, the deformations at the connections may overcome the limits reported in the literature. This observation points to the need to develop specific regulations to access existing buildings of this typology. The nonlinear analysis carried out showed that static procedures appear to underestimate the seismic demand.

The development of reliable numerical models is of critical importance to carry out analysis at a local or larger scale. Making use of the information gathered about the Portuguese buildings, hundreds of nonlinear numerical models, representative of the existing building stock, were generated in an automatized manner through simulated design. The fragility curves derived, reflecting the probability of achieving a given limit state given a certain intensity measure, e.g., spectral acceleration, showed that large structural and non-structural damage is expected for moderate levels of seismic intensity. As observed for the existing buildings, this apparent vulnerability results essentially from the high slenderness of the columns, which reaches its maximum lateral strength for very low levels of lateral load. Even in the building typologies that do not feature steel dowels at the beam-to-column connections, only a small portion of the buildings (around 15%) presented structural issues at the connections.

The fragility analysis was further used to carry out, for the first time, an estimation of the direct and indirect losses considering the population of Portuguese PRC buildings. This analysis revealed a distinct outcome for the two scenarios considered, with losses for the offshore scenario (representative of the 1755 Lisbon Earthquake) significantly higher than the ones associated with the onshore case (representative of the Tagus River valley). Accordingly, the estimated losses can reach nearly 1% of the national GDP for the offshore event, which is 10 times higher than the losses estimated for the onshore scenario. These values were determined under the assumption that the PRC buildings represent only approximately 12% of the total industrial building stock. The disaggregation of the losses showed that the indirect losses (business interruption and the disruption in the economy) could reach values larger than the direct impact. The latter are mainly associated with nonstructural damage and the losses in the contents and inventory, which points to the need to take mitigation measures to minimize these vulnerabilities.

9. Project Publications

Journal Publications

C. Raposo, F. Rodrigues, H. Rodrigues, "BIM-based LCA assessment of seismic strengthening solutions for reinforced concrete precast industrial buildings", Innovative Infrastructure Solutions, 4(1), 2019. doi:10.1007/s41062-019-0239-7

N. Batalha, H. Rodrigues, and H. Varum, "Seismic performance of RC precast industrial buildings — learning with the past earthquakes", Innovative Infrastructures Solutions, vol. 4, 2019. doi:10.1007/s41062-018-0191-y

R. Sousa, N. Batalha, and H. Rodrigues, "Numerical simulation of beam-to-column connections in precast reinforced concrete buildings using fibre-based frame models", Engineering Structures, vol. 203, 2020. doi:10.1016/j.engstruct.2019.109845

H. Rodrigues, R. Sousa, N. Batalha, H. Vitorino, H. Varum, and P. Fernandes, "Characterization of Portuguese RC precast industrial building stock", Advances in Civil Engineering, 2020. doi:10.1155/2020/7517205

N. Batalha, R. Sousa, H. Vitorino, H. Varum, P. Fernandes, and H. Rodrigues, "Modelação do comportamento sísmico de edifícios pré-fabricados de betão armado", Revista Portuguesa de Engenharia de Estruturas, 2020.

R. Sousa, N. Batalha, V. Silva, and H. Rodrigues, "Seismic fragility functions for Portuguese RC precast buildings", Bulletin of Earthquake Engineering, 2020. doi:10.1007/s10518-020-01007-7

H. Rodrigues, H. Vitorino, N. Batalha, R. Sousa, P. Fernandes, H. Varum, "Influence of the beam-to-column connection in the Seismic Performance of Precast Concrete industrial facility", Structural Engineering International, 2021. doi:10.1080/10168664.2021.1920082

L. Ostetto, R. Sousa, H. Rodrigues, and P. Fernandes, "Assessment of the seismic behavior of a precast reinforced concrete industrial building with the presence of horizontal cladding panels", Buildings, 11(9), 400, 2021. doi:10.3390/buildings11090400

N. Batalha, H. Rodrigues, A. Arêde, A. Furtado, R. Sousa, and H. Varum, "Cyclic behaviour of precast beam-to-column connections with low seismic detailing", Earthquake Engineering and Structural Dynamics, 2022. doi:10.1002/eqe.3606

Conference Papaers

N. Batalha, H. Rodrigues, H. Varum, P. Fernandes, and R. Sousa, "Comportamento sísmico de um pavilhão pré-fabricado de betão armado", 11º Congresso Nacional de Sismologia e Engenharia Sísmica, Lisboa, 2019.

N. Batalha, H. Rodrigues, and H. Varum, "Seismic assessment of an industrial precast RC buildings", 3rd Doctoral Congress in Engineering, Porto, 2019.

R. Sousa, N. Batalha, and H. Rodrigues, "Review of strategies for modelling beam-to-column connections in existing precast industrial RC buildings", Congresso de Métodos Numéricos em Engenharia, Guimarães, 2019.

H. Vitorino, N. Batalha, R. Sousa, P. Fernandes, H. Varum, and H. Rodrigues, "Assessment of Seismic behavior of a RC Precast building", Conferece on Automation Innovation in Construction, Leiria, 2019.

N. Batalha, H. Rodrigues, A. Arêde, A. Furtado, R. Sousa, and H. Varum, "Caracterização experimental de ligações pré-fabricadas em betão armado sob ações cíclicas",12º Congresso Nacional de Mecânica Experimental, Leiria, 2020.

N. Batalha, H. Rodrigues, A. Arêde, A. Furtado, R. Sousa, and H. Varum, "Simulação numérica do reforço de uma ligação viga-pilar de edifícios industriais pré-fabricados em betão armado", CONREA, Aveiro, 2021.

N. Batalha, H. Rodrigues, R. Sousa, H. Varum, and P. Fernandes, "Assessment of existing RC Precast industrial buildings according with Eurocode 8 – Part 3", Fib Symposium, Lisbon, 2021.

L. Ostetto, R. Sousa, H. Rodrigues, and P. Fernandes, "Analysis of the influence of cladding panels in the seismic behaviour of a PRC Industrial Buildings", Fib Symposium, Lisbon, 2021.

R. Sousa, N. Batalha, H. Rodrigues, V. Silva, P. Fernandes, and H. Varum, "Seismic Fragility of Precast RC Buildings in Portugal", World Conference on Earthquake Engineering, Sendai, Japan, 2021.

R. Sousa, N. Batalha, V. Silva, P. Fernandes, H. Varum, and H. Rodrigues, "Curvas de fragilidade para edifícios industriais pré-fabricados em betão armado em Portugal", Reabilitar & Betão Estrutural, Lisbon, Portugal, 2021.

10.

References

[1] P. M. D. R. Lagartixo, "Sistemas Estruturais de Edifícios Industriais Pré-Fabricados em Betão," Faculdade de Ciências e Tecnologia da Universidade Nova de Lisboa, 2011.

[2] A. Belleri, E. Brunesi, R. Nascimbene, M. Pagani, and P. Riva, "Seismic performance of precast industrial facilities following major earthquakes in the Italian territory," J. Perform. Constr. Facil., pp. 1–31, 2015.

[3] H. Sezen and A. Whittaker, "Seismic Performance of Industrial Facilities Affected by the 1999 Turkey Earthquake," J. Perform. Constr. Facil., no. February, pp. 28–36, 2006.

[4] L. Liberatore, L. Sorrentino, D. Liberatore, and L. Decanini, "Failure of industrial structures induced by the Emilia (Italy) 2012 earthquakes," Eng. Fail. Anal., vol. 34, pp. 629–647, 2013.

[5] G. Magliulo, M. Ercolino, C. Petrone, O. Coppola, and G. Manfredi, "The Emilia earthquake: Seismic performance of precast reinforced concrete buildings," Earthq. Spectra, vol. 30, no. 2, pp. 891–912, 2014.

[6] D. Bournas, P. Negro, and F. F. Taucer, "Performance of industrial buildings during the Emilia earthquakes in Northern Italy and recommendations for their strengthening," Bull. Earthq. Eng., vol. 12, no. 5, pp. 2383–2404, 2013.

[7] C. Demartino, I. Vanzi, and G. Monti, "Precast industrial buildings in Southern Europe : loss of support at frictional beam-to-column connections under seismic actions," Bull. Earthq. Eng., vol. 16, no. 1, pp. 259–294, 2018.

[8] F. Cornali, A. Belleri, A. Marini, and P. Riva, "Influence of modelling assumptions in the expected loss evaluation of a precast industrial building," Procedia Eng., vol. 199, pp. 3510–3515, 2017.

[9] X. Romão et al., "Field observations and interpretation of the structural performance of constructions after the 11 May 2011 Lorca earthquake," Eng. Fail. Anal., vol. 34, pp. 670–692, 2013.

[10] R. Nascimbene, "Numerical Model of a Reinforced Concrete Building : Earthquake Analysis and Experimental Validation," pp. 521–530, 2015.

[11] R. M. Oinam Romanbabu, A. Kumar, and R. Sahoo Dipti, "Cyclic performance of steel fiber-reinforced concrete exterior beam-column joints," Earthquakes Struct., vol. 16, no. 5, pp. 533–546, May 2019.

[12] R. M. Oinam, D. R. Sahoo, and R. Sindhu, "Cyclic Response of Non-ductile RC Frame with Steel Fibers at Beam-Column Joints and Plastic Hinge Regions," J. Earthq. Eng., vol. 18, no. 6, pp. 908–928, Aug. 2014.

[13] H. Rodrigues, X. Romão, A. Andrade-Campos, H. Varum, A. Arêde, and A. G. Costa, "Simplified hysteretic model for the representation of the biaxial bending response of RC columns," Eng. Struct., vol. 44, 2012.

[14] M. Posada and S. Wood, "Seismic Performance of Precast Industrial Buildings in Turkey," 7th U.S. Natl. Conf. Earthq. Eng., no. August 1999, p. 10, 2002.

[15] F. Minghini, E. Ongaretto, V. Ligabue, M. Savoia, and N. Tullini, "Observational failure analysis of precast buildings after the 2012 Emilia earthquakes," Earthq. Struct., vol. 11, no. 2, pp. 327–346, 2016.

[16] N. Batalha, H. Rodrigues, and H. Varum, "Seismic performance of RC precast industrial buildings — learning with the past earthquakes," Innov. Infrastruct. Solut., vol. 4, no. 4, pp. 1–13, 2019.

[17] M. H. Arslan and H. H. Korkmaz, "What is to be learned from damage and failure of reinforced concrete structures during recent earthquakes in Turkey?," Eng. Fail. Anal., vol. 14, pp. 1–22, 2007.

[18] C. Casotto, V. Silva, H. Crowley, R. Pinho, and R. Nascimbene, "Scenario damage analysis of RC precast industrial structures in Tuscany, Italy," in Second European conference on earthquake engineering and seismology, 2014, pp. 1–12.

[19] M. Savoia, N. Buratti, and L. Vincenzi, "Damage and collapses in industrial precast buildings after the 2012 Emilia earthquake," Eng. Struct., vol. 137, pp. 162–180, 2017.

[20] B. Zoubek, "Estimation of the cyclic capacity of beam-to-column dowel connections in precast industrial buildings," Bull. Earthq. Eng., vol. 13, no. 7, pp. 2145–2168, 2014.

[21] C. Casotto, V. Silva, H. Crowley, R. Nascimbene, and R. Pinho, "Seismic fragility of Italian RC precast industrial structures," Eng. Struct., vol. 94, pp. 122–136, 2015.

[22] FEMA, "Seismic Considerations for Steel Storage Racks," 2005.

[23] B. Dal Lago, S. Bianchi, F. Biondini, and G. Toniolo, "Dissipative diaphragm connections for precast structures with cladding panels under seismic action," in 16th European Conference on Earthquake Engineering, 2018, pp. 1–12.

[24] E. Del, M. Cesare, F. Sonia, B. Giovanni, and M. Orlando, "An innovative cladding panel connection for RC precast buildings," Bull. Earthq. Eng., vol. 17, no. 2, pp. 845–865, 2019.

[25] H. Rodrigues, R. Sousa, H. Vitorino, N. Batalha, H. Varum, and P. Fernandes, "Characterisation of Portuguese RC Precast Industrial Building Stock," Adv. Civ. Eng., pp. 1–19, 2020.

[26] B. Zoubek, M. Fischinger, and T. Isakovic, "Cyclic response of hammer-head strap cladding-to-structure connections used in RC precast building," vol. 119, pp. 135–148, 2016.

[27] M. Ercolino, G. Magliulo, and O. Coppola, "Code formula for the fundamental period of RC precast buildings."

[28] M. Menegotto, "Observations on precast concrete structures of industrial buildings and warehouses," Progett. sismica (Special issue 2009 L'Aquila earthquake), vol. 3, pp. 149–153, 2009.

[29] CEN, Eurocode 8: Design of structures for earthquake resistance. Part 1: general rules, seismic actions and rules for buildings. Brussels, Belgium, 2004.

[30] CEN, "Eurocode 8: Design of structures for earthquake resistance. Part 3: Assessment and retrofitting of buildings. EN 1998-3, Comité Européen de Normalisation," Brussels, Belgium, 2005.

[31] A. Braconi et al., "Prefabricated steel structures for low-rise buildings in seismic areas (Precasteel)," Brussels, 2013.

[32] FFMS, "Número de empresas de industrias transformadoras," Pordata, 2017. .

[33] C. Chastre and V. Lúcio, Estruturas Pré-moldadas no Mundo - Aplicações e Comportamento Estrutural, Fundação d. 2012..

[34] D. Beilic, C. Casotto, R. Nascimbene, D. Cicola, and D. Rodrigues, "Seismic fragility curves of single storey RC precast structures by comparing different Italian codes," Earthquakes Struct., vol. 12, no. 3, pp. 359–374, Jan. 2017.

[35] B. Zoubek, T. Isakovic, Y. Fahjan, and M. Fischinger, "Cyclic failure analysis of the beam-to-column dowel connections in precast industrial buildings," Eng. Struct., vol. 52, pp. 179–191, 2013.

[36] H. Rodrigues, R. Sousa, N. Batalha, H. Vitorino, H. Varum, and P. Fernandes, "Typical properties of the Portuguese precast industrial buildings," Adv. Civ. Eng., 2020.

[37] R. Sousa, N. Batalha, and H. Rodrigues, "Numerical simulation of beam-to-column connections in precast reinforced concrete buildings using fibre-based frame models," Eng. Struct., vol. 203, 2020.

[38] Z. Zhang, S. Wang, and J. Feng, "Frictional behaviour of the interface between concrete and rubber : Laboratory shear test and its elastoplastic model," Eng. Fract. Mech., vol. 197, no. April, pp. 192–205, 2018.

[39] F. Clementi, A. Scalbi, and S. Lenci, "Seismic performance of precast reinforced concrete buildings with dowel pin connections," J. Build. Eng., vol. 7, pp. 224–238, 2016.

[40] G. Magliulo, G. Fabbrocino, and G. Manfredi, "Seismic assessment of existing precast industrial buildings using static and dynamic nonlinear analyses," Eng. Struct., vol. 30, no. 9, pp. 2580–2588, 2008.

[41] H. M. Elsanadedy, T. H. Almusallam, Y. A. Al-salloum, and H. Abbas, "Investigation of precast RC beam-column assemblies under column-loss scenario," Constr. Build. Mater., vol. 142, pp. 552–571, 2017.

[42] D. Feng, G. Wu, and Y. Lu, "Finite element modelling approach for precast reinforced concrete beam-to-column connections under cyclic loading," Eng. Struct., vol. 174, no. May, pp. 49–66, 2018.

[43] M. Kataoka, M. Ferreira, and A. Debs, "Nonlinear FE analysis of slab-beam-column connection in precast concrete structures," Eng. Struct., vol. 143, pp. 306–315, 2017.

[44] I. N. Psycharis and H. P. Mouzakis, "Shear resistance of pinned connections of precast members to monotonic and cyclic loading," Eng. Struct., vol. 41, pp. 413–427, 2012.

[45] D. A. Bournas, P. Negro, and F. J. Molina, "Pseudodynamic tests on a full-scale 3-storey precast concrete building : Behavior of the mechanical connections and floor diaphragms," Eng. Struct., vol. 57, pp. 609–627, 2013.

[46] M. Araújo, L. Macedo, M. Marques, and J. M. Castro, "Code-based record selection methods for seismic performance assessment of buildings," Earthq. Eng. Struct. Dyn., pp. 129–148, 2016.

[47] H. Rodrigues, R. Sousa, H. Vitorino, N. Batalha, H. Varum, and P. Fernandes, "Characterisation of Portuguese RC Precast Industrial Building Stock," Adv. Civ. Eng., pp. 1–19, 2020.

[48] "NP EN 1992-1-1:2010, Eurocódigo 2 –Projeto de Estruturas de Betão –Parte 1-1: Regras gerais e regras para edifícios," Instituto Português da Qualidade.

[49] F. McKenna, "OpenSees: A Framework for Earthquake Engineering Simulation," Comput. Sci. Eng., vol. 13, no. 4, pp. 58–66, 2011.

[50] M. Menegotto and P. E. Pinto, "Method of analysis for cyclically loaded reinforced concrete plane frames including changes in geometry and non-elastic behaviour of elements under combined normal force and bending," in IABSE symposium of resistance and ultimate deformability of structures, Lisbon, Portugal, 1973, pp. 5–22.

[51] P. Fajfar, "A Nonlinear Analysis Method for Performance Based Seismic Design," Earthq. Spectra, vol. 16, no. 3, pp. 573–592, 2000.

[52] Eurocódigo, "Eurocódigo 8: Projecto de estruturas para resistência aos sismos," pp. 1–226, 2009.

[53] A. Belleri and P. Riva, "Horizontal cladding panels : in-plane seismic performance in precast concrete buildings," Bull. Earthq. Eng., vol. 14, no. 4, pp. 1103–1129, 2016.

[54] B. A. Bradley, R. P. Dhakal, M. Cubrinovski, G. A. MacRae, and D. S. Lee, "Seismic loss estimation for efficient decision making," Bull. New Zeal. Soc. Earthq. Eng., vol. 42, no. 2, pp. 96–110, Jun. 2009.

[55] V. Silva, H. Crowley, H. Varum, and R. Pinho, "Seismic risk assessment for mainland Portugal," Bull. Earthq. Eng., vol. 13, no. 2, pp. 429–457, Feb. 2015.

[56] L. Sousa, "Risco Sísmico em Portugal Continental," Instituto Superior Técnico, 2006.

[57] J. M. C. Estêvão et al., "Earthquake resilient schools in Algarve (Portugal) and Huelva (Spain)," 16th Eur. Conf. Earthq. Eng., 2018.

[58] V. Silva, H. Crowley, M. Pagani, D. Monelli, and R. Pinho, "Development of the OpenQuake engine, the Global Earthquake Model's open-source software for seismic risk assessment," Nat. Hazards J. Int. Soc. Prev. Mitig. Nat. Hazards, vol. 72, no. 3, pp. 1409–1427, 2014.

[59] M. Pagani et al., "Openquake engine: An open hazard (and risk) software for the global earthquake model," Seismol. Res. Lett., vol. 85, no. 3, pp. 692–702, 2014.

[60] V. Silva and N. Paul, "Potential impact of earthquakes during the 2020 COVID-19 pandemic," Earthq. Spectra, vol. 37, no. 1, pp. 73–94, 2020.

[61] H. Crowley et al., "Exposure model for European seismic risk assessment:," https://doi.org/10.1177/8755293020919429, vol. 36, no. 1_suppl, pp. 252–273, Jun. 2020.

[62] L. Sousa, V. Silva, and P. Bazzurro, "Using open-access data in the development of exposure data sets of industrial buildings for earthquake risk modeling," Earthq. Spectra, vol. 33, no. 1, pp. 63–84, 2017.

[63] FEMA, "Multi-hazard Loss Estimation Methodology – Earthquake Model: HAZUS®MH. Advanced engineering building module – Technical and user's manual," vol. 2, 2003.

[64] INE, "Estatísticas da Produção Industrial - 2019," Inst. Nac. Estatística, I. P., p. 41, 2020.

[65] R. Sousa, N. Batalha, V. Silva, and H. Rodrigues, "Seismic fragility functions for Portuguese RC precast buildings," Bull. Earthq. Eng. 2020, pp. 1–18, Nov. 2020.

[66] A. Furtado, C. Costa, A. Arêde, and H. Rodrigues, "Geometric characterisation of Portuguese RC buildings with masonry infill walls," Eur. J. Environ. Civ. Eng., vol. 20, no. 4, 2016.

[67] V. Silva, H. Crowley, H. Varum, R. Pinho, and L. Sousa, "Investigation of the characteristics of Portuguese regular moment-frame RC buildings and development of a vulnerability model," Bull. Earthq. Eng., vol. 13, no. 5, pp. 1455–1490, 2015.

[68] RSA, "Regulamento de Segurança e Acções para Estruturas de Edifícios e Pontes - Decreto-Lei n.o 235/83." 1983.

[69] P. Fajfar, "Capacity spectrum method based on inelastic demand spectra," Earthq. Eng. Struct. Dyn., vol. 28, no. 9, pp. 979–993, Sep. 1999.

[70] A. Ozerdem and S. Barakat, "After the Marmara earthquake : Lessons for avoiding short cuts to disasters," no. September 2014, 2000.

[71] INE, "Sistema Integrado de Matrizes Simétricas Input-Output 2013," Inst. Nac. Estatística, I. P., 2017.

[72] H. Rodrigues, H. Vitorino, N. Batalha, R. Sousa, P. Fernandes, and H. Varum, "Influence of Beam-to-Column Connections in the Seismic Performance of Precast Concrete Industrial Facilities," https://doi.org/10.1080/10168664.2021.1920082, 2021.

[73] K. Nasserasadi and M. Ghafory-Ashtiany, "Major Contributing Factors to Seismic Risk of Industrial Facilities," in Proceedings of the 14 World Conference on Earthquake Engineering, 2008.

Seismic Precast ///

Cofinanciado por:

COMPETE 2020

PORTUGAL 2020

UNIÃO EUROPEIA
Fundos Europeus Estruturais e de Investimento